Low-lying bending vibronic bands of the MgNC $\tilde{A}\,^2\Pi - \tilde{X}\,^2\Sigma^+$ transition

Masaru Fukushima[a] and Takashi Ishiwata
Faculty of Information Sciences, Hiroshima City University, Hiroshima 731-3194, Japan

(Received 12 March 2007; accepted 21 May 2007; published online 30 July 2007)

We have generated MgNC in supersonic free jet expansions and measured the laser induced fluorescence excitation spectra of the Mg–N–C bending vibronic bands of the $\tilde{A}\,^2\Pi - \tilde{X}\,^2\Sigma^+$ transition. In addition to the two vibronic bands, 2_0^1, $\kappa\,^2\Sigma^{(+)}$- and 2_0^2, $\kappa\,^2\Pi - ^2\Sigma^+$, reported previously, the 2_0^2, $\mu\,^2\Pi_{1/2} - ^2\Sigma^+$ vibronic subband was found just above the 2_0^1 band. The most remarkable feature of this subband is unexpected rotational structure of the $\tilde{A}$ (020) $\mu\,^2\Pi_{1/2}$ level, showing the splitting of the *e* and *f* sublevels. On the basis of the fact that the $\tilde{A}$ (020) $\mu\,^2\Pi_{1/2}$ level lies very close to the $\tilde{A}$ (010) $\kappa^2\Sigma^{(+)}$ level, the *e*/*f* splitting is ascribed to *P*-type doubling which is induced by Coriolis interaction between these two bending vibronic levels. Introducing the Coriolis coupling terms arising from the **G**-uncoupling operator, $-J^{\pm}G_{22}^{\mp}$, and the spin-Coriolis interaction, $S^{\pm}G_{22}^{\mp}$, into the rotational Hamiltonian, this unexpected rotational structure has been analyzed. This *P*-type doubling would be one of the rare examples exhibiting the Coriolis interaction between two bending vibronic levels with $\Delta v_2 = \pm 1$ and $\Delta l = \mp 1$. Through the molecular constants of the $\tilde{A}$ (010) $\kappa\,^2\Sigma^{(+)}$, (020) $\kappa\,^2\Pi$, and $\mu\,^2\Pi_{1/2}$ levels, the Renner-Teller vibronic structure of the ν_2 bending mode in the $\tilde{A}\,^2\Pi$ state has been characterized. The observed vibronic bands analyzed in this study show some anomalies in the band intensities. Based on the information of the ν_2 bending vibronic structure derived from the present analyses, we discuss the intensity anomalies. © *2007 American Institute of Physics*. [DOI: 10.1063/1.2748769]

I. INTRODUCTION

MgNC is one of the milestone molecules among about 150 of the interstellar species observed so far, since it was the first Mg-containing species identified among them.[1,2] In spite of the substantial cosmic abundance of Mg, the Mg-containing species had not been observed in interstellar space for a while. In 1986, a millimeter-wave spectrum was observed from the circumstellar envelope of the star IRC +10216, but the spectral carrier could not be assigned at that time.[2] The carrier was identified as MgNC in 1993, when the observation of the rotational spectrum of the species succeeded in the laboratory, being led by a prediction of the molecular structure in quantum chemical calculation.[1]

The electronic spectrum of the $\tilde{A}\,^2\Pi - \tilde{X}\,^2\Sigma^+$ transition of MgNC was first reported by Wright and Miller using the laser induced fluorescence (LIF) technique.[3] The reported spectrum was in the region from the origin band, 0_0^0, to the fundamental vibronic band of the Mg–NC stretching (ν_3) mode, 3_0^1, which was about 580 cm^{-1} above the origin band. They analyzed the rotational structure of the 0_0^0 and 3_0^1 vibronic bands. The Mg–N–C bending (ν_2) vibronic bands were also analyzed by taking the Renner-Teller and spin-orbit interactions into account. We have extended the observations and identified the 1_0^1 band lying at about 2000 cm^{-1} above the origin band. The rotationally resolved electronic spectra of the C–N stretching (ν_1) vibronic bands, 1_0^1 and $1_0^1 3_0^1$, were then analyzed.[4] Based on the molecular constants obtained, we discussed the fine structure of the $\tilde{A}\,^2\Pi$ state. The vibronic structure of the $\tilde{A}\,^2\Pi$ state of MgNC was studied through theoretical and computational chemistry.[5–7] Quantum chemical studies were carried out on the vibronic structures of the ground $\tilde{X}\,^2\Sigma^+$ state of MgNC and both of the $\tilde{A}$ and $\tilde{X}$ states of MgCN.[8–10] The permanent electric dipole moments of both the ground $\tilde{X}\,^2\Sigma^+$ and excited $\tilde{A}\,^2\Pi$ states of MgNC were determined by Steimle and Bousquet utilizing the optical Stark spectroscopy.[11]

Recently, we have obtained the electronic spectrum lying between the regions reported by Wright and Miller[3] and studied in our previous work.[4] In this spectral region, some new vibronic bands attributed to the $\tilde{A}\,^2\Pi - \tilde{X}\,^2\Sigma^+$ electronic transition of MgNC were identified. Among them, the stretching bands in the spectrum have been reported previously.[12] In this paper, we focus our attention on the analyses of the low-lying vibronic bands of the ν_2 mode, 2_0^1 and 2_0^2, and discuss an anomaly observed in the rotational structure of the 2_0^2 $\mu\,^2\Pi_{1/2}$ vibronic level; i.e., an unexpectedly large *e*/*f* splitting of the rotational lines. On the basis of the molecular constants obtained, we will also discuss the Renner-Teller structure of the $\tilde{A}\,^2\Pi$ state.

II. EXPERIMENT

The details of the experimental setup have been given in our previous papers.[4,12] The MgNC free radicals were generated by the laser ablation technique under the supersonic

[a]Author to whom correspondence should be addressed. Electronic mail: fukushim@im.hiroshima-cu.ac.jp

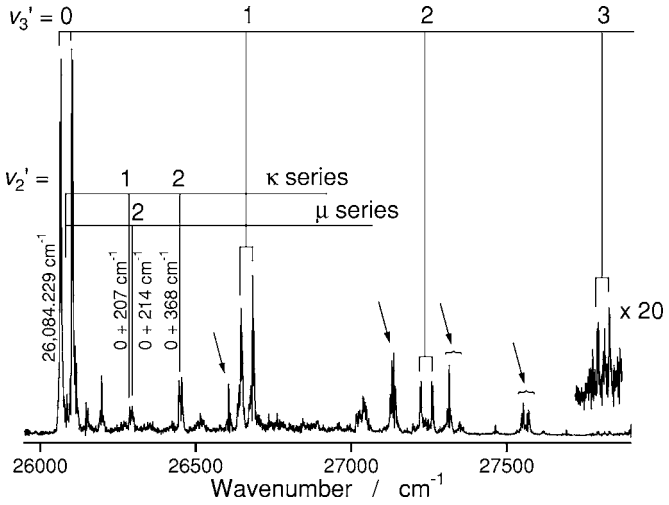

FIG. 1. The LIF excitation spectrum of MgNC observed in the supersonic free jet expansions of Ar. In this work, our interest is focused on the three ν_2 bending vibronic bands indicated by vertical lines. The transition energies of these bands are indicated by using the energy distances from the 0_0^0 band, 26 084.229 cm^{-1}, such as 0+207 cm^{-1} for the band observed at 26 290 cm^{-1}. The progression of the ν_3 stretching vibronic bands analyzed in our previous manuscript is also indicated in the spectrum (Ref. 12). The four vibronic bands of the $\tilde{A}\,^2\Pi - \tilde{X}\,^2\Sigma^+$ transition of MgOH are indicated by arrows.

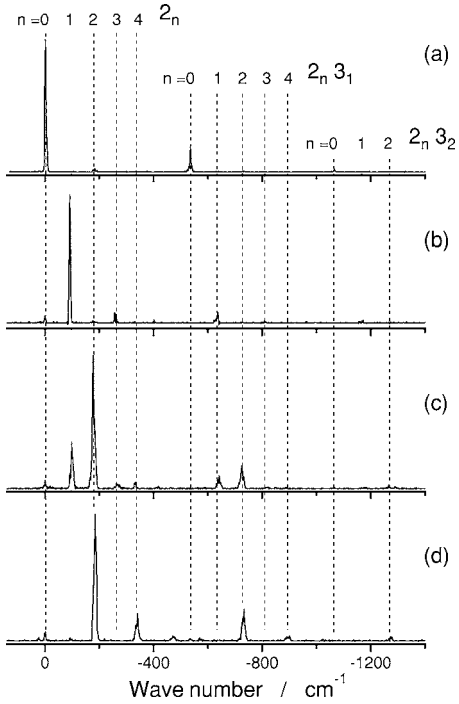

FIG. 2. The dispersed fluorescence spectra obtained by the excitation of the vibronic bands of the ν_2 vibrational progression shown in Fig. 1: (a) 0_0^0, $\Omega=\frac{1}{2}$, (b) 2_0^1 $\kappa\,^2\Sigma^{(+)}$ (0+207 cm^{-1}), (c) 2_0^2 $\mu\,^2\Pi$ (0+214 cm^{-1}), and (d) 2_0^2 $\kappa\,^2\Pi$ (0+368 cm^{-1}). The horizontal scale indicates the energy distance from the excitation laser wave number in each spectrum.

free jet expansion condition. Using a pulsed valve (General Valve, Series 9), Ar gas containing acetonitrile (CH_3CN) at the saturated vapor pressure of about −25 °C was expanded into the vacuum with a stagnation pressure of ~1 atm. Synchronized with the pulsed gas flow, the second harmonics of a pulsed Nd^{3+} YAG (yttrium aluminum garnet) laser were irradiated on the metallic Mg surface which was placed just downstream of the valve orifice. The MgNC radicals were generated in an Ar plasma produced by the laser ablation of Mg, and were injected into the vacuum with the Ar gas flow. At 40 mm downstream from the laser vaporization point, the LIF signals were observed by the excitation of the second harmonics output of a pulsed Nd^{3+} YAG laser pumped dye laser (Spectra Physics, Quanta-Ray PRO-250 and Lambda Physik, Scanmate 2E). The energy resolution of the UV probe laser was about 0.2 cm^{-1}, and its frequency was calibrated with optogalvanic lines of Ne for the red fundamental output. To achieve higher energy resolution, an étalon could be inserted in the laser cavity. The resolution was then improved to be about 0.03 cm^{-1}, and the laser frequency was calibrated by reference to the absorption spectrum of I_2 for the fundamental output. The LIF signals were treated by a gated integrator (Stanford Research, SR-245) and normalized against the probe laser power at each shot. Magnesium rod (High Purity Chemetals Laboratory, 99.9%), acetonitrile (Katayama Chemical, Special Grade), and Ar (Nippon Sanso, Research Purity) were used without further purification.

III. RESULTS

Figure 1 shows the overview of our spectrum observed in the energy region below the ν_1 fundamental band, 1_0^1. It was measured under the lower resolution condition using the dye of LDS-751 (Styryl 8) as the laser medium. Some of the vibronic bands were assigned to the ν_3 stretching vibronic progression, 3_0^n, $n=0-3$, as indicated in the figure, and have been analyzed previously.[3,12] The other bands lying between 0_0^0 and 3_0^1 bands are assigned to the ν_2 bending vibronic bands.

Figure 2 shows the dispersed fluorescence spectra obtained by the excitation of the 0_0^0 band and the bands lying at 207, 214, and 368 cm^{-1} above the 0_0^0 band. The dispersed spectra show a progression with vibrational interval starting with ~93 cm^{-1}, as indicated by dashed lines in the spectra. Because this interval is in quite good agreement with the value predicted for the vibrational energy of the ν_2 bending mode, e.g., 110.8 cm^{-1} (Refs. 4 and 12) and 94.0 cm^{-1},[8] the progression is assigned to that of the ν_2 bending mode. On this basis, the vibronic bands in the excitation spectrum are attributed to the ν_2 bending vibronic bands. The strongest vibronic band in each dispersed spectrum is $v_2''=0$, 1, 2, and 2 for the 0_0^0 band, 0+207, 0+214, and 0+368 cm^{-1} bands, respectively. It would be expected that the identical potential surface approximation seems to be valid for the ν_2 bending modes in the $\tilde{A}\,^2\Pi$ and $\tilde{X}\,^2\Sigma^+$ states, because similar vibrational frequencies are predicted; 157.1 and 110.8 cm^{-1} for the ν_2 bending vibrational frequency of the $\tilde{A}\,^2\Pi$ and $\tilde{X}\,^2\Sigma^+$ states, respectively.[4,12] Because the equilibrium geometries of these states are linear, it would be deduced from this approximation that the $\Delta v_2=0$ transition occurs as the strongest band in each of the dispersed spectra. Accordingly, the 0+207, 0+214, and 0+368 cm^{-1} bands in the excitation spectrum are attributed to the ν_2 vibronic bands assigned as the 2_0^1, 2_0^2, and 2_0^2 transitions, respectively, as denoted in Fig. 1. These assignments are consistent with the rotational analysis

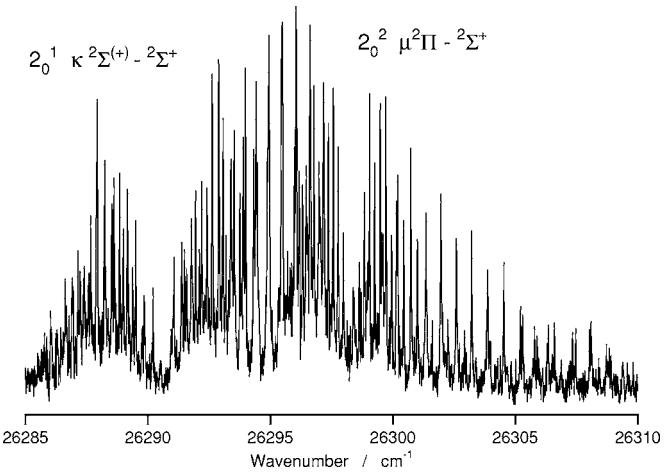

FIG. 3. The rotationally resolved LIF excitation spectrum of the bending vibronic bands, 2_0^1 $\kappa\,^2\Sigma^{(+)}-{}^2\Sigma^+$ and 2_0^2 $\mu\,^2\Pi_{1/2}-{}^2\Sigma^+$.

of these bands described in the following subsections. The vibrational structure of the $\tilde{X}\,^2\Sigma^+$ state occurring in the dispersed spectra will be discussed in a separate paper.[13]

A. The $\tilde{A}$ (010) $\kappa\,^2\Sigma^{(+)}-\tilde{X}$ (000) $^2\Sigma^+$ band

The rotationally resolved spectrum of the 2_0^1, $\kappa\,^2\Sigma^{(+)}-{}^2\Sigma^+$ band at ~26 290 cm^{-1} is shown in Fig. 3. [Hereafter, we abbreviate the 2_0^1, $\kappa\,^2\Sigma^{(+)}-{}^2\Sigma^+$ band as 2_0^1 $\kappa\,^2\Sigma^{(+)}$, because all of the spectra described henceforth in this paper have the vibrationless ground electronic state $^2\Sigma^+$ as the lower state in common.] In this spectrum, we can notice that another vibronic band at ~26 298 cm^{-1}, which is assigned to 2_0^2 from the dispersed fluorescence spectra, lies just above the 2_0^1 band. This band will be attributed to the 2_0^2 $\mu\,^2\Pi_{1/2}$ band unambiguously, as discussed in Sec. III C. It should be noted that the 2_0^1 $\kappa\,^2\Sigma^{(+)}$ band is the transition with $\Delta l=\pm 1$, contrary to the selection rule of $\Delta l=0$, and is interpreted as a forbidden component of a dipole allowed $^2\Pi-{}^2\Sigma^+$ electronic transition in a linear molecule. The intensity of this band is thought to be induced through Herzberg-Teller vibronic interaction with other electronic states. However, the transition intensity of this forbidden band is anomalously strong, being comparable to the allowed transitions, and we need to consider a local perturbation, as described in Sec. IV C.

The rotational structure of the 2_0^1, $\kappa\,^2\Sigma^{(+)}$ band shows a typical pattern of a parallel band observed in a $^2\Sigma-{}^2\Sigma$ transition.[14] To analyze the rotational structure, the following Hamiltonian has been used for the ground $^2\Sigma^+$ state:

$$H = H_{\rm rot} + H_{\rm SR},$$

where $H_{\rm rot}$ is the molecular rotational Hamiltonian with centrifugal distortion terms, and $H_{\rm SR}$ is the spin-rotation Hamiltonian. Since the term of $H_{\rm SR}$ was reported to be small as compared with the energy resolution of our experimental apparatus[1,15] this term was neglected in the present analysis. To evaluate the matrix element, we adopted Hund's case (a) basis function for the lower vibronic levels,

$$|v_2,l;J,M_J,P,\Lambda,S,\Sigma\rangle = |v_2,l\rangle|J,M_J,P\rangle|\Lambda\rangle|S,\Sigma\rangle.$$

The matrix elements of the Hamiltonians for these basis functions were cited from Refs. 16 and 17.

For the upper (010) $\kappa\,^2\Sigma^{(+)}$ vibronic level, we followed the formulation proposed by Hougen.[18] We adopted the formulation in the J expression under the limiting case condition of $r \gg B_{\rm eff}^{\kappa\Sigma} J$,

$$F(\kappa\,^2\Sigma,J) = T_v^{\kappa\Sigma} + B_{\rm eff}^{\kappa\Sigma} J(J+1) \pm \tfrac{1}{2} p^{\kappa\Sigma}\left(J+\tfrac{1}{2}\right), \quad (1)$$

where the upper and lower signs refer to the e and f sublevels (or the F_1 and F_2 components), respectively, $T_v^{\kappa\Sigma}$ is the band origin, $B_{\rm eff}^{\kappa\Sigma}$ is the effective rotational constant, and $p^{\kappa\Sigma}$ is a constant for the e/f splitting. In this paper, the two sublevels in the $^2\Sigma^{(+)}$ level are classified as those with e and f parities, though they are usually distinguished as two spin sublevels, F_1 and F_2. The superscript $\kappa\Sigma$ is attached to the constants to clarify the upper vibronic level. In the limiting condition, r expresses a convenient parameter to describe the influence of the spin-orbit and Renner-Teller interactions which will be described in Sec. IV A. Briefly, the limiting condition of $r \gg B_{\rm eff}^{\kappa\Sigma} J$ means that the strengths of the Renner-Teller and/or spin-orbit interactions are much larger than the energy separation from the adjacent rotational level. The expression, Eq. (1), corresponds to the lower-order rotational level energy expression for the $^2(\frac{1}{2})$ $(=^{2S+1}(\Omega))$ state of case (c) molecules including the Ω-type doubling [or to that for the $^2\Pi_{1/2}$ state of the case (a) molecules including the Λ-type doubling],[19] and thus the $p^{\kappa\Sigma}$ constant corresponds to the Ω-type doubling constant of the $^2(\frac{1}{2})$ electronic state. We will discuss the interpretation of the $p^{\kappa\Sigma}$ constant and the validity of the limiting condition in Sec. IV A. In this J expression, the $^2\Sigma^{(+)}-{}^2\Sigma$ vibronic transition is treated as in the same way as a $^2(\frac{1}{2})-{}^2\Sigma$ electronic transition. As mentioned by Hougen, the level energy can also be represented in N expression. The N expression is similar to the more familiar form known for the rotational energy level expression of the $^2\Sigma$ electronic state with non-negligible spin splitting. However, we take the J expression rather than the N expression, since we will need to consider the interaction between the rotational levels of the (010) $\kappa\,^2\Sigma^{(+)}$ and (020) $\mu\,^2\Pi$ vibronic levels following the $\Delta J=0$ selection rule later. Since the p constant in the J expression has a simple relation with γ in the N expression, $p=2B-\gamma$, as usual in the case of $^2\Sigma$ electronic states,[18] we can compare our p constant with the γ constant.

On the basis described above, the rotational structure of the observed spectrum was reasonably analyzed, as the assignments of the observed lines are listed in the supplement.[20] The molecular constants thus obtained are listed in Table I. Here it is better to mention that the $p^{\kappa\Sigma}$ constant in the upper $^2\Sigma^{(+)}$ vibronic level is unexpectedly larger than the value which would be expected from the Ω-type doubling constant in the $^2(\frac{1}{2})$ state of a case (c) electronic state. This larger separation results from the fact that the $^2\Sigma^{(+)}$ level is a $^2\Sigma$ vibronic level in the $\tilde{A}\,^2\Pi$ electronic state caused by the Renner-Teller and spin-orbit interactions.[18] To reveal the large $p^{\kappa\Sigma}$ constant, the term values of the $\tilde{A}$ (010) $\kappa\,^2\Sigma^{(+)}$ rotational levels are shown in

TABLE I. Molecular parameters obtained from the rotational analysis of the $\tilde{A}(010)\kappa\,^2\Sigma^{(+)}-\tilde{X}(000)^2\Sigma^+$ band of MgNC (numbers in parentheses are one standard deviation in units of the last significant digit) (in cm^{-1}).

	This work	Ref. 3
	The $\tilde{A}\,^2\Pi$ state	
$B_{\rm eff}^{\kappa\Sigma}$	0.204 90(2)	0.205 09(6)
$p^{\kappa\Sigma}$	0.359 3(3)	⋯
γ	0.050 5[a]	0.049 6(2)
$T_{v'}^{\kappa\Sigma}$	26 290.641(2)	26 290.59(1)[b]
	The $\tilde{X}\,^2\Sigma^+$ state	
B_0''	0.199 034 476[c]	0.199 01(4)[d]

[a]The value calculated from the $B'_{\rm eff}$ and p constants obtained.
[b]The definition might be different from ours. See text.
[c]Fixed to the value obtained through global fit (Ref. 15) of the millimeter wave (Ref. 1) and FTMW (Ref. 15).
[d]The value of the 0_0^0 band.

Fig. 4. The rotational structure of this band has been previously analyzed by Wright and Miller, using the N expression.[3] For comparison, we evaluate the γ constant using the relation with the p constant, and we confirm that the derived value is consistent with their constant within 3σ, as seen in Table I.

B. The $\tilde{A}$ (020) $\kappa\,^2\Pi-\tilde{X}$ (000) $^2\Sigma^+$ band

The rotationally resolved spectrum of the $\tilde{A}$ (020) $\kappa\,^2\Pi-\tilde{X}$ (000) $^2\Sigma^+$ band is shown in Fig. 5. The rotational structure of this band shows a typical pattern of the case (a) $^2\Pi-^2\Sigma$ transition consisting of two spin components.[14] The structure looks similar to that of the 0_0^0 and the Mg–NC and C–N stretching vibronic bands.[3,4,12] However, the energy spacing between the band origins of the $P=\frac{1}{2}$ and $=\frac{3}{2}$ spin components is much narrower than those of the 0_0^0 and stretching bands (P should be replaced by Ω in the stretching bands), which prevents the simultaneous analysis of the two

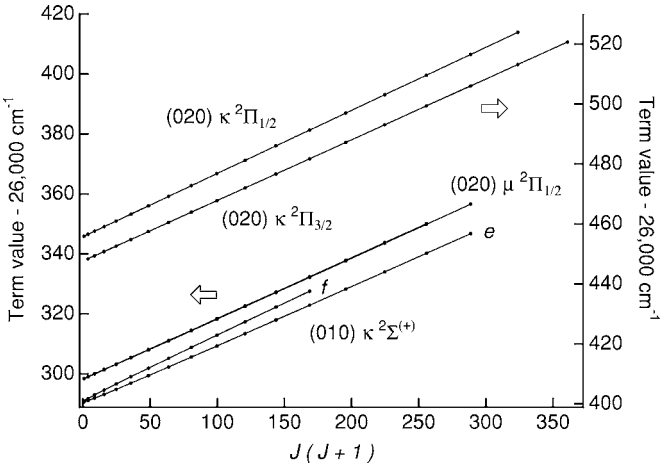

FIG. 4. The term values of the vibronic levels of the $\tilde{A}\,^2\Pi$ state, plotted as functions of $J(J+1)$. The dots represent the energies of experimentally observed levels. The energies of the (010) $\kappa\,^2\Sigma^{(+)}$ and (020) $\mu\,^2\Pi_{1/2}$ levels should be referred to the left axis and that for (020) $\kappa\,^2\Pi$ level should be ascribed to the right. The (020) $\mu\,^2\Pi_{1/2}$ vibronic level shows e/f parity splitting (see Fig. 7 in detail).

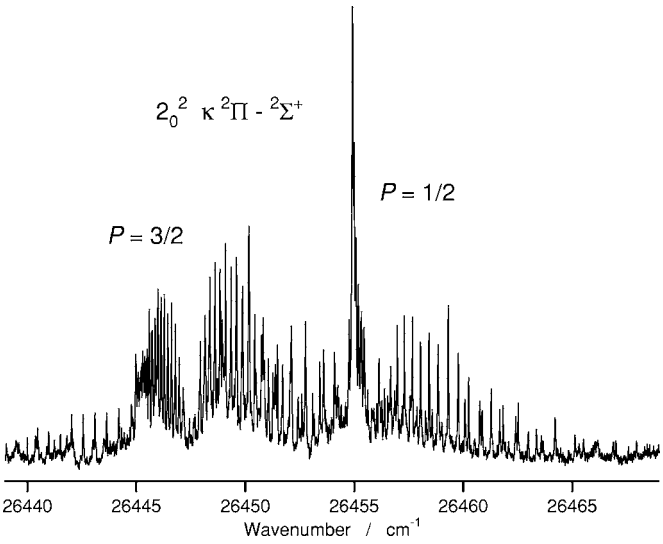

FIG. 5. The rotationally resolved LIF excitation spectrum of the bending vibronic band, $2_0^2\ \kappa\,^2\Pi-^2\Sigma^+$.

spin components of the $2_0^2\ \kappa\,^2\Pi$ band. We thus analyzed the P components independently, which is the same procedure that we called a tentative analysis in the study of the C–N stretching bands.[4] In this procedure, the same Hamiltonian and basis function as those employed in Sec. III A have been used for the vibrationless vibronic level of the ground $^2\Sigma^+$ electronic state.

For the upper (020) $\kappa^2\Pi$ vibronic level, the effective Hamiltonian used is as follows:

$$H = H_{\rm rot} + H_{\rm SO} + H_{\rm SR} + H_{\rm LD},$$

where $H_{\rm rot}$ and $H_{\rm SR}$ are the same as those used in the ground $^2\Sigma^+$ state, $H_{\rm SO}$ represents the spin-orbit interaction, and $H_{\rm LD}$ represents the Λ-type doubling. Since two spin components were analyzed separately, any information on the $H_{\rm SO}$ term was not concerned. Furthermore, the spin-rotation and Λ-type doubling terms were ignored, since the splitting of the e/f parity sublevels has not been observed.[4,12] To evaluate the matrix elements, we adopted Hund's case (a) basis functions mentioned in Sec. III A. The matrix elements of the Hamiltonian in the basis functions were cited from Refs. 16 and 17. The Hamiltonian matrix thus derived is essentially the same as Hougen's formulation for the $0\neq K\neq v_2+1$ vibronic levels under the limiting case of $r\gg|w|$, $r\gg B_{\rm eff}^{\kappa\Pi_P}J$ and $|w|\gg B_{\rm eff}^{\kappa\Pi_P}J$,[18] where $B_{\rm eff}^{\kappa\Pi_P}$ is the effective rotational constant of the $\kappa\,^2\Pi$ vibronic level. We analyze each spin component using the following equations:

$$\begin{aligned} F(\kappa\,^2\Pi_{1/2},J) &= T_v^{\kappa\Pi_{1/2}} + B_{\rm eff}^{\kappa\Pi_{1/2}}J(J+1), \\ F(\kappa\,^2\Pi_{3/2},J) &= T_v^{\kappa\Pi_{3/2}} + B_{\rm eff}^{\kappa\Pi_{3/2}}J(J+1), \end{aligned} \tag{2}$$

where $T_v^{\kappa\Pi_P}$ is the band origin. We attach the superscript $\kappa\Pi_P$ to the constants to clarify the upper vibronic level.

Analyzing the two spin components independently, we obtained good results for the rotational analysis of the 2_0^2 $\kappa\,^2\Pi$ vibronic level. The assignments of the observed lines

TABLE II. Molecular parameters obtained from the rotational analysis of the $\tilde{A}(020)\kappa\,^2\Pi-\tilde{X}(000)^2\Sigma^+$ band of MgNC (numbers in parentheses are one standard deviation in units of the last significant digit) (in cm^{-1}).

	This work			
	$P=\frac{1}{2}$	$P=\frac{3}{2}$	Ave.	Ref. 3
	The $\tilde{A}\,^2\Pi$ state			
$B_{\rm eff}^{\kappa\Pi_P}$	0.210 60(2)	0.202 43(2)	0.2065[a]	0.2071(1)
$\bar{A}$[b]	⋯	⋯	−8.178	⋯
A[c]	⋯	⋯	⋯	−8.138(4)
$T_{v'}^{\kappa\Pi_P}$	26 455.749(3)	26 447.571(3)	26 451.660[d]	26 451.57(1)
	The $\tilde{X}\,^2\Sigma^+$ state			
B_0''	0.199 034 476[e]			0.199 01(4)[f]

[a]Average between the constants of the $P=\frac{1}{2}$ and $=\frac{3}{2}$ levels.
[b]The $\bar{A}$ constant; i.e., the distance between the $P=\frac{1}{2}$ and $=\frac{3}{2}$ levels. $\bar{A}=T_{2_0^2}\kappa\,^2\Pi_{1/2}-T_{2_0^2}\kappa\,^2\Pi_{3/2}$.
[c]The spin-orbit constant, A.
[d]Average between the band origins of the $P=\frac{1}{2}$ and $=\frac{3}{2}$ levels.
[e]Fixed to the value obtained through global fit (Ref. 15) of the millimeter wave (Ref. 1) and FTMW (Ref. 15).
[f]The value of the 0_0^0 band.

are listed in the supplement,[20] and the molecular constants obtained are listed in Table II. The term values of the upper (020) $\kappa\,^2\Pi_{1/2}$ and $^2\Pi_{3/2}$ rotational levels are also shown in Fig. 4 in addition to those of (010) $\kappa\,^2\Sigma^{(+)}$. The average of our rotational constants of the two spin components, $\bar{B}_{\rm eff}$ $\left(=\frac{1}{2}(B_{\rm eff}^{\kappa\Pi 1/2}+B_{\rm eff}^{\kappa\Pi 3/2})\right)$ is in good agreement with the corresponding B value reported by Wright and Miller,[3] and the spacing between the two band origins, $\bar{A}$ $(=T_v^{\kappa\Pi_{1/2}}-T_v^{\kappa\Pi_{3/2}})$, is found to be close to their spin-orbit interaction constant. From the lowest rotational level observed in each spectrum, the higher and lower spin components are assigned to the $P=\frac{1}{2}$ and $=\frac{3}{2}$, respectively. This energy ordering of the P components is usual in a $\kappa\,^2\Pi$ vibronic level with positive Renner parameter, ϵ, while it is inverted in a $\mu\,^2\Pi$ vibronic level, which is the partner of the κ level in the Renner-Teller splitting. Although Wright and Miller reported the same conclusion as ours for the energy ordering of the P components, they assigned this band to the (020) $\mu\,^2\Pi$ vibronic band by assuming the second-order homogeneous interaction of the μ vibronic level with the $\tilde{X}\,^2\Sigma^+$ electronic state.[3] However, this band should be assigned to the (020) $\kappa\,^2\Pi$ vibronic level, as we will discuss the Renner-Teller structure of the $\tilde{A}\,^2\Pi$ state in Sec. IV A.

Here we would like to note a problem which we met in our previous work.[12] The spin-orbit interaction constants derived for the upper vibronic levels of the 0_0^0 and 3_0^1 stretching vibronic bands, A, showed distinct discrepancies with those reported by Wright and Miller.[3] However, it should be pointed out that the spacings between the band origins of two spin-orbit components, $\bar{A}$, were equivalent to their spin-orbit interaction constants for these upper levels. Our constants satisfied a well-known relationship derived by Hill and Van Vleck;[21] $\bar{A}=A-2B$ for $^2\Pi$ electronic states of case (a), where $\bar{A}$ is the spacing between the two band origins of the two spin components following Kroto.[16]

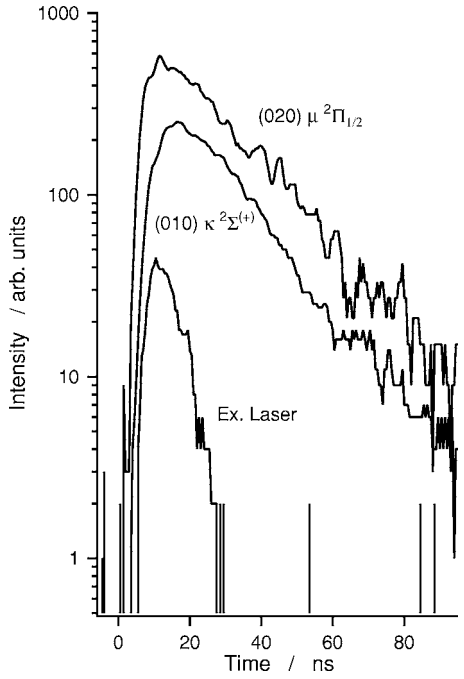

FIG. 6. The time profiles of the fluorescence from the 2^1 $\kappa\,^2\Sigma^{(+)}$ and 2^2 $\mu\,^2\Pi_{1/2}$ vibronic levels and of the excitation light source.

The situation is quite similar in the analysis of the $\kappa\,^2\Pi$ vibronic level under study. We obtain the effective rotational constants for the two P components of the $\kappa\,^2\Pi$ vibronic level, $B_{\rm eff}^{\kappa\Pi 1/2}$ and $B_{\rm eff}^{\kappa\Pi 3/2}$, whose average is consistent with the rotational constant derived by Wright and Miller,[3] while the separation between two P components, $\bar{A}$, is equivalent to their spin-orbit interaction constant, A. Hill and Van Vleck's relationship should fail in the bending $^2\Pi$ vibronic level, because the Renner-Teller vibronic interaction induced by the vibrational angular momentum also contributed to the energy splitting between the $P=\frac{1}{2}$ and $=\frac{3}{2}$ components. It is thus difficult to derive the spin-orbit interaction constant from the analysis of the $\kappa\,^2\Pi$ vibronic level alone. Wright and Miller seem to use the same procedure in analyzing the vibrationless level as well as the bending and stretching vibronic levels. As we conjectured,[12] it would be speculated that their A constant would not be A in their Hamiltonian but $\bar{A}$.[12] Unfortunately, we cannot compare our observed rotational transition frequencies with Wright and Miller's, since we have not been able to obtain the frequency lists of the observed lines.

C. The $\tilde{A}$ (020) $\mu\,^2\Pi_{1/2}-\tilde{X}$ (000) $^2\Sigma^+$ band

There is a vibronic band lying just above the 2_0^1 $\kappa\,^2\Sigma^{(+)}$ band, as shown in Fig. 3. In the spectrum of the 2_0^1 $\kappa\,^2\Sigma^{(+)}$ band reported by Wright and Miller, a part of this band is found, but they did not recognize this band as a vibronic band of MgNC.[3] The fluorescence lifetimes of the vibronic levels of the $\tilde{A}\,^2\Pi$ state are about 15 ns as shown in Fig. 6, which shows the time profile of the fluorescence from the 2^1 $\kappa\,^2\Sigma^{(+)}$ vibronic level as an example. The fluorescence

TABLE III. Molecular parameters obtained from the rotational analysis of the $\tilde{A}(020)\mu\,^2\Pi_{1/2}-\tilde{X}(000)\,^2\Sigma^+$ band of MgNC (numbers in parentheses are one standard deviation in units of the last significant digit) (in cm^{-1}).

	e	f	Ave.[a]	e/f[b]
	The $\tilde{A}\,^2\Pi$ state			
$B_{\rm eff}^{\mu\Pi_{1/2}}$	0.1997(1)	0.2008(1)	0.2002	0.200 16(8)
D'	$9.0(5)\times10^{-6}$	$7.0(4)\times10^{-6}$	8.0×10^{-6}	$8.0(3)\times10^{-6}$
β	⋯	⋯	⋯	−0.016 2(4)
$T_{v'}^{\mu\Pi_{1/2}}$	26 298.200(6)	26 298.269(4)	26 298.235	26 298.237(4)
	The $\tilde{X}\,^2\Sigma^+$ state			
B_0''[c]	0.199 034 476			0.199 034 476

[a]Average between the constants of the e and f sublevels.
[b]The constants obtained from the analysis using Eq. (6).
[c]Fixed to the value obtained through global fit (Ref. 15) of the millimeter wave (Ref. 1) and FTMW (Ref. 15).

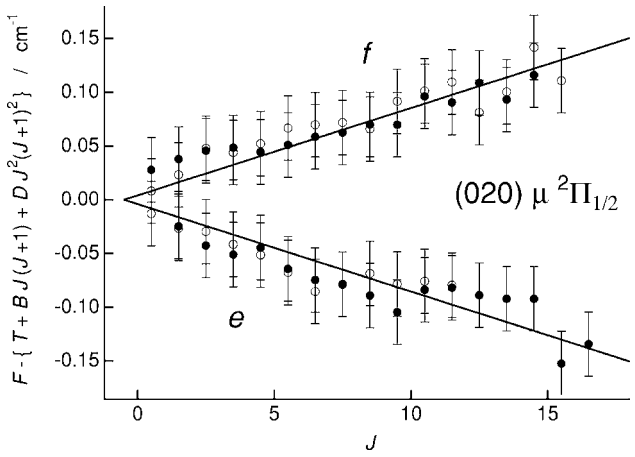

FIG. 7. The e/f displacements of the (020) $\mu\,^2\Pi_{1/2}$ vibronic level of the $\tilde{A}\,^2\Pi$ state, plotted as functions of J. The open and closed circles represent the level energies obtained from the P and R branches, respectively, and the error bars indicate the resolution of our probe laser. The full lines show the level energies calculated from the $\beta^{\mu\Pi}$ constants determined in this study.

lifetime of the new vibronic level is also determined to be about 15 ns, as shown in Fig. 6 for comparison. As indicated by dotted lines in Fig. 2, the dispersed fluorescence spectrum observed by the excitation of this band, spectrum (c), shows a progression whose vibrational intervals are identical to those observed by the excitation at the other frequencies in spectra (a), (b), and (d). Based on these findings, it is concluded that the spectral species of this band is the same as that of the other bands, and we attribute it to a vibronic band of the $\tilde{A}\,^2\Pi-\tilde{X}\,^2\Sigma^+$ electronic transition of MgNC.

Spectrum (c) in Fig. 2 has the transition to the $v_2''=2$ level as the strongest band, and we ascribed it to the $2_0^2\,\mu\,^2\Pi$ band. The other 2_0^2 vibronic band assigned to $2_0^2\,\kappa\,^2\Pi$ lies at the higher energies, as described Sec. III B. One of the remarkable features of the $2_0^2\,\mu\,^2\Pi$ vibronic band is that we have been able to observe only one of the two P components. The observed component will be attributed to the $P=\frac{1}{2}$ component in view of its rotational structure as described later, and the other spin component of $P=\frac{3}{2}$ has not been identified even with careful examination [unassigned weak lines lying between 26 305 and 26 310 cm^{-1} in the spectrum may be attributed to the transitions to the $\frac{3}{2}$ component, because the energy separation of them from the band origin of $2_0^2\,\mu\,^2\Pi_{1/2}$ is close to that between the $P=\frac{1}{2}$ and $=\frac{3}{2}$ components in the (020) $\kappa\,^2\Pi$ level, ~8 cm^{-1}]. To analyze the rotational structure of the $2_0^2\,\mu\,^2\Pi_{1/2}$ band, we first applied the same procedure as the $2_0^2\,\kappa\,^2\Pi$ band, since the rotational structure looks similar to that of the one of the two components of the 2_0^2 $\kappa\,^2\Pi$ band, as shown in Fig. 5. But this analysis failed due to unexpectedly large splitting between the e and f sublevels in the upper (020) $\mu\Pi_{1/2}$ vibronic level. The e and f sublevels were thus analyzed independently. The molecular constants obtained are listed in Table III, and the term values of the e and f sublevels are plotted in Fig. 7. Since the lowest observed rotational line is $J=\frac{1}{2}$, the upper level is assigned to be the $P=\frac{1}{2}$ component of the (020) $\mu\,^2\Pi$ vibronic level of the $\tilde{A}\,^2\Pi$ state.

The feature of the e/f splitting is quite similar to that of the Λ-type doubling of a $^2\Pi_{1/2}$ electronic state caused by heterogeneous interaction with a remote $^2\Sigma^+$ state; the energy separation between the e and f sublevels is proportional to $\left(J+\frac{1}{2}\right)$ expected for the Λ-type doubling in the $\Omega=\frac{1}{2}$ level under the case (a) limit.[19] However, the doubling of the 2_0^2 $\mu\,^2\Pi_{1/2}$ band cannot be explained by the Λ-type doubling in the usual $^2\Pi$ electronic state, because the (020) $\kappa\,^2\Pi$ vibronic level, which is the partner of the $\mu\,^2\Pi$ level in the Renner-Teller splitting, does not show the doubling. In the bending vibronic level, the Λ-type doubling due to a heterogeneous interaction with a remote $^2\Sigma$ electronic state is expected to occur in both of the κ and μ components.

The term values of the upper (020) $\mu\,^2\Pi_{1/2}$ rotational levels are also shown in Fig. 4 in addition to those of (010) $\kappa\,^2\Sigma^{(+)}$ and (020) $\kappa\,^2\Pi$. They are calculated using the constants of the ground state listed in Table III. It is easily recognized that the (020) $\mu\,^2\Pi_{1/2}$ vibronic level lies quite close to the (010) $\kappa\,^2\Sigma^{(+)}$ vibronic level. Thus, it is likely that the e/f splitting of the (020) $\mu\,^2\Pi_{1/2}$ level is induced by the accidental proximity with the $\kappa\,^2\Sigma^{(+)}$ vibronic level lying only by 8 cm^{-1} lower. Being different from the electronically induced Λ-type doubling (or the K-type doubling in the present case) described by the **L**- and **S**-uncoupling operators and the spin-orbit and spin-electronic interaction terms, the e/f splitting of the (020) $\mu\,^2\Pi_{1/2}$ vibronic level is thought to be a vibronically induced P-type doubling described by the **G**-uncoupling operator and spin-vibration coupling term.

For a ν_2 bending vibronic level of a $^2\Pi$ electronic state, the rotational Hamiltonian is expressed as follows:

$$H_{\rm rot}=B\boldsymbol{R}^2=B(\boldsymbol{J}-\boldsymbol{L}-\boldsymbol{S}-\boldsymbol{G})^2. \tag{3}$$

Within the approved framework in the vibration-rotation interaction of linear molecule, the $\boldsymbol{G}$ operator has the diagonal element, $G^z|v_2,l\rangle=l|v_2,l\rangle$, and the eights of the off diagonal, $G^{\pm}$, with $\Delta v_2=\pm1$, $\Delta l=\pm1$, and $\Delta v_k=\pm1$, where $k=1$ or 3.[22] In the present case, since $\Gamma(02^00)\otimes\Gamma(01^10)\otimes\Gamma(R_a)$ is a totally symmetric irreducible representation, the Coriolis coupling between the (020) $^2\Pi$ and (010) $^2\Sigma^{(+)}$ vibronic levels is considerable, though it is not included in $\boldsymbol{G}$ under the traditional theoretical framework. The vibrational angular momentum operator for the pure ν_2 bending vibronic levels,

which presents the Coriolis coupling, is expressed here as $\boldsymbol{G}_{22}$. As described in Eq. (A2), there are four kinds of the off-diagonal operator with $\Delta v_2 = \pm 1$ and $\Delta l = \pm 1$, G_{22}^{+}, G_{22}^{-}, $G_{22}^{+\dagger}$, and $G_{22}^{-\dagger}$, for the vibrational angular momentum operator, $\boldsymbol{G}_{22}$, in addition to the diagonal, $G_{22}^{z}|v_2,l\rangle = l|v_2,l\rangle$. In analogy with $\boldsymbol{G}$ in Eq. (3), the $\boldsymbol{G}_{22}$ term corresponds to the lowest order Coriolis term in the vibration-rotation Hamiltonian, $\boldsymbol{J}\boldsymbol{\pi}$; i.e., $\boldsymbol{G}_{22}$ is classified into the $\boldsymbol{Jpq}$ element of Table 6.4 in Kroto's book.[16,23] In the present case, we can adapt Eq. (3) by replacing $\boldsymbol{G}$ with $\boldsymbol{G}_{22}$, and apply the following rotational Hamiltonian to the present analysis:

$$H_{\mathrm{rot}} = B\boldsymbol{R}^2 = B(\boldsymbol{J} - \boldsymbol{L} - \boldsymbol{S} - \boldsymbol{G}_{22})^2. \tag{4}$$

Under the case (a) limit, the off-diagonal term of $-J^{\pm}G_{22}^{\mp}$, which could be called as the **G**-uncoupling operator, can heterogeneously couple the (020) $\mu\ ^2\Pi_{1/2}$ vibronic level with (010) $\kappa\ ^2\Sigma^{(+)}$, and induces different effects on e and f parity sublevels. In addition to the $-J^{\pm}G_{22}^{\mp}$ term, the spin-vibration interaction described by the off-diagonal term of $S^{\pm}G_{22}^{\mp}$ can also couple these two vibronic levels homogeneously. The interactions induced by the $\boldsymbol{G}$-uncoupling operator and spin-vibration coupling are classified in the Coriolis interaction, and the e/f splitting under the study is considered to be a sort of P-type doubling caused by the Coriolis interaction. The evaluation of the P-type doubling is similar to that of the Λ-type doubling, where the **S**-uncoupling operator, $-J^{\pm}S^{\mp}$, is necessary to take into account. The **S**-uncoupling operator describes the heterogeneous ($\Delta\Omega = \pm 1$) interaction effective between the $^2\Pi_{1/2}$ and $^2\Pi_{3/2}$ vibronic levels. However, in the present case, the S-uncoupling term is not included in the analysis, because there is no trace of the interaction in the (020) $\kappa\ ^2\Pi$ vibronic levels. The e/f splitting is therefore evaluated as the doubling caused by the Coriolis interaction between the closely lying (020) $^2\Pi_{1/2}$ and (010) $^2\Sigma^{(+)}$ vibronic levels. Accounting for these two interaction terms by the Van Vleck transformation,[16,22]

$$H' = B(-J^{\pm}G_{22}^{\mp} + S^{\pm}G_{22}^{\mp}), \tag{5}$$

we can obtain the following expression for the energy level of the (020) $^2\Pi_{1/2}$ as described in the Appendix:

$$F(\mu\ ^2\Pi_{1/2}, J) = T_v^{\mu\Pi_{1/2}} + B_{\mathrm{eff}}^{\mu\Pi_{1/2}} J(J+1) \mp \tfrac{1}{2}\beta^{\mu\Pi}\left(J + \tfrac{1}{2}\right), \tag{6}$$

where the upper and lower signs refer to the e and f sublevels, respectively, $T_v^{\mu\Pi_{1/2}}$ is the band origin, and $B_{\mathrm{eff}}^{\mu\Pi_{1/2}}$ is the effective rotational constant. The superscript $\mu\Pi_{1/2}$ is added to the constants to clarify the upper vibronic level. The last term corresponds to that arising from the Coriolis interaction described in Eq. (5). The rotational structure of the observed spectrum was then reasonably analyzed, as the assignments of the spectral lines are listed in the supplement.[20] The molecular constants obtained are listed in Table III. Here the centrifugal distortion term, $D'\{J(J+1)\}^2$, was included in the analysis, though we omitted it in Eq. (6) for simplicity. The D' constant obtained is very tiny but necessary to reproduce the observed term values.

IV. DISCUSSION

A. The vibronic structure of the $\tilde{A}\ ^2\Pi$ electronic state

After the pioneering work by Renner,[24] the Renner-Teller interaction has been one of the subjects of theoretical works.[18,25–27] Among them, the most fundamental work on the $^2\Pi$ electronic state is that by Hougen,[18] in the situation of which we need to take account of not only the Renner-Teller interaction but also the spin-orbit interaction. To describe these interactions, Hougen introduced two convenient parameters, r and β, depending on v_2 and K. As shown in Fig. 8(a), the r and β parameters denote the total strength of the Renner-Teller and spin-orbit interactions and the ratio between the strength of these interactions, respectively,

$$2r = \sqrt{A^2 + R^2},$$

$$\tan 2\beta = \frac{R}{A}, \tag{7}$$

$$R = \epsilon\omega_2\sqrt{(v_2+1)^2 - K^2}.$$

As shown in Fig. 8(a), the relation between the two parameters and the magnitudes of the two interactions is understood as something like one between the polar and Cartesian coordinates. By combining the use of these two, r and β, with the w and C parameters, the energy levels of the $(0v_20)$, $v_2 = 0-2$, vibronic states under the limiting case of $r \gg BJ$, as shown in Fig. 8(b). The additional parameters there introduced are defined as follows:

$$w = -CK\cos 2\beta,$$

$$C = -\tfrac{1}{8}(v_2+1)\epsilon^2\omega_2,$$

$$C' = -\tfrac{1}{8}(v_2+1)(v_2+2)\epsilon^2\omega_2,$$

where the C' parameter corresponds to the C parameter of the nondegenerate vibronic level with $K = v_2 + 1$, so-called unique level.[26]

Based on the energy diagram in Fig. 8(b), we can evaluate the vibronic parameters using the observed band origins of the four vibronic bands, 0_0^0, $2_0^1\ \kappa\ ^2\Sigma^{(+)}$, $2_0^2\ \mu\ ^2\Pi$, and $2_0^2\ \kappa\ ^2\Pi$. The constants obtained by a least-squares fitting are listed in the column, Analysis I, of Table IV, and the deviations of the vibrational energies of the fitting are shown in the column, Analysis I, of Table V. In the analysis, we fixed the A constant to the value derived from the 0_0^0 band,[12] because of its strong correlation to the Renner-Teller parameter ϵ within the available information. The deviations are much larger than our experimental accuracy. Thus we introduced the anharmonic term into the vibronic energies, though the vibronic levels treated are low-lying bending levels in which the anharmonicity is usually not remarkable. A few works have been carried out about the theoretical analysis of the anharmonic term.[28–31] They showed that there are two factors giving the anharmonicity of the bending vibronic structure. One arises from anharmonicity of the bending potential which is characterized by the anharmonic potential parameters, g_4 and $\hat{g}_4$. The other comes from the dipolar vibronic

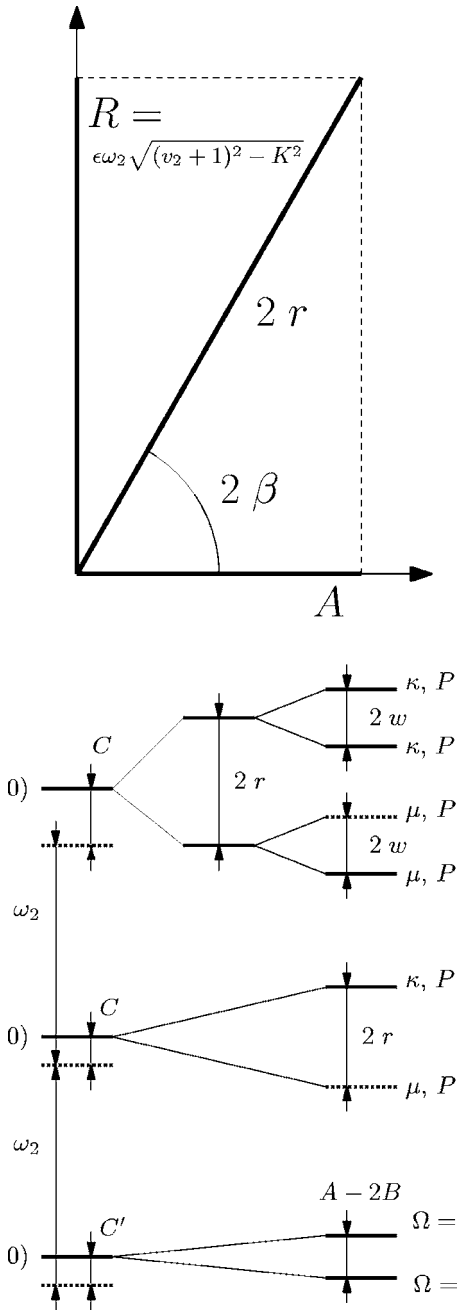

FIG. 8. (a) A diagram showing the relation among the vibronic molecular parameters. (b) A diagram showing the Renner-Teller vibronic structure of the low-lying bending vibronic levels of the $\tilde{A}\,^2\Pi$ state. In the right hand side, the solid lines indicate the vibronic levels observed in this experiment, while the dashed ones denote unobserved levels. For simplicity, the Σ and Π vibronic levels with $K=0$ and =1, respectively, are only displayed in (b). The $K=2$ levels, which are not to be observed in this study, are involved in the $v_2=1$ vibronic levels. The parameters r, β, w, C, and C' have the v_2 and K dependence. See text for details.

coupling with other electronic states which is described by the vibronic parameter, g_K. We adopted the anharmonic correction proposed by Brown and Jørgensen; Eq. (8.3) in Ref. 31. Here, we have $g_4=\hat{g}_4$, assuming that the quartic anharmonic constant is the same for both bending potentials. Due to the restricted data, we cannot include two parameters into the analysis simultaneously and consider them separately. The results including g_K in the analysis are shown in the columns, Analysis II, in Tables IV and V, and those for $g_4(=\hat{g}_4)$ are in the columns, Analysis III, of the tables. These parameters improve the fitting evidently, but it is obvious that the anharmonic parameter, g_4, is more effective than the vibronic, g_K. We thus take Analysis III as our final result.

The anharmonic parameters are expressed as $g_4=\frac{1}{24}\phi_{2222}$ and $\hat{g}_4=\frac{1}{24}\hat{\phi}_{2222}$, where ϕ_{2222} and $\hat{\phi}_{2222}$ are the quartic force constants of the bending mode.[30] The negative value of the anharmonic parameter, g_4, indicates that the bending potential surface widens with increase of energy. The isomerization reaction barrier in the $\tilde{A}\,^2\Pi$ state is predicted to be low; 1940 and 809 cm^{-1} for the A' and A'' surfaces from the bottom of the MgNC isomer, respectively.[9] The importance of the negative anharmonic parameter in these low-lying bending levels is consistent with the prediction. The x_{22} constant is expressed as

$$x_{22,s}=\frac{3}{2}\frac{g_4+s\hat{g}_4}{1+s\epsilon}+\frac{1}{16}\sum_{k=1,3}\phi_{k22,s}^2\left\{\frac{\omega_k}{4\omega_{2,s}^2-\omega_k^2}-\frac{2}{\omega_k}\right\},$$

where the $\phi_{k22,s}$ is the cubic force constant, and k represents the stretching mode, ν_1 or ν_3. The value s is +1 for the upper potential and is −1 for the lower.[30] When $\omega_2 \ll \omega_k$, the second term is reduced to be $-\frac{3}{16}\Sigma\,\phi_{k22}{}^2\omega_{k^{-1}}$ and can be negligible as compared to the first term, since ω_1 and ω_3 are reported to be 2051.3 and 584.6 cm^{-1}, respectively.[12] From $g_4=-1.8$ cm^{-1} determined, x_{22} is evaluated to be −3.9 cm^{-1} which is consistent with $x_{22}=-3.1$ cm^{-1} predicted from calculations.[5] It would imply that the anharmonicity of the bending potential gives more predominant effect than the vibronic coupling with the $\tilde{X}\,^2\Sigma^+$ state in the vibronic structure of the $\tilde{A}\,^2\Pi$ state.

Table IV summarizes the vibronic constants reported previously in the experimental[3] and computational works.[8] By Wright and Miller, the 2_0^2 $\kappa\,^2\Pi$ vibronic band was assigned to 2_0^2 $\mu\,^2\Pi$ instead, as mentioned in Sec. III B, and accordingly their constants show remarkable differences from ours. In contrast, the predictions from computational works are consistent with our results. On the basis of the constants determined in this study, it is confirmed that the limiting conditions, $r \gg |w|$, $r \gg B^{\kappa\Sigma}J$, $|w| \gg B^{\kappa\Sigma}J$, etc., which we assumed in analyzing the spectra, are satisfied in the present system.

From the spectral analysis, we could only derive the absolute value of the Renner parameter ϵ. The sign has not been determined, because ϵ always appeared as ϵ^2 in describing the Renner-Teller effect. When a linear molecule bends, the degenerate bending potential splits into two, V^+ and V^-, where the index denotes the parity of the defining electronic wave function under a reflection in the molecular plane.[32] The sign of ϵ indicates which potential is more stable than the other under the bending motion. The ϵ constant is defined by

$$\epsilon=\frac{V^+-V^-}{V^++V^-}=\frac{\omega_+^2-\omega_-^2}{\omega_+^2+\omega_-^2},$$

where ω_+ and ω_- are the harmonic bending frequencies for the V^+ and V^- potentials, respectively. As Mg–N–C bends, the highest occupied molecular orbital of the $\tilde{A}\,^2\Pi$ electronic

TABLE IV. The vibronic constants of the $\tilde{A}\,^2\Pi$ state of MgNC (numbers in parentheses are one standard deviation in units of the last significant digit)(cm^{-1}).

	This work				
	Analysis I[a]	Analysis II[a]	Analysis III[a]	Ref. 3	Calc.
ω_2 (cm^{-1})	146(1)	143.5(9)	153.6(6)	193	157.1,[b] 163.4[c]
g_K (cm^{-1})	⋯	−8.0(19)	⋯	⋯	⋯
g_4[d] (cm^{-1})	⋯	⋯	−1.8(2)	⋯	⋯
ϵ	0.353(8)	0.361(3)	0.396(4)	0.05	0.259[c]
A (cm^{-1})	37.372[e]	37.372[e]	37.372[e]	36.926[f]	34.85[c]

[a]See text.
[b]Value predicted by Fukushima and Ishiwata (Ref. 4).
[c]Value predicted by Odaka *et al.* (Ref. 5)
[d]$g_4=\hat{g}_4$.
[e]Fixed.
[f]The A constant of the vibrationless level.

state, 3π, splits into symmetric a' and antisymmetric a'' orbitals. From the Walsh diagram, the antisymmetric a'' orbital is predicted to be stabilized more than a', and the relation $\omega_+ > \omega_-$ is derived. A positive value of ϵ would be therefore expected for the $\tilde{A}\,^2\Pi$ electronic state.

For the (020) κ and μ $^2\Pi$ vibronic levels in a $^2\Pi$ electronic state, Hougen evaluated the following expressions to the B_{eff} terms involved in Eqs. (2) and (6):

$$B_{\text{eff}}^{\kappa\Pi} = B\left\{1 + \frac{B}{2r}\cos^2 2\beta \pm \frac{B}{2|w|}\sin^2 2\beta\right\},$$
$$B_{\text{eff}}^{\mu\Pi} = B\left\{1 - \frac{B}{2r}\cos^2 2\beta \pm \frac{B}{2|w|}\sin^2 2\beta\right\}, \quad (8)$$

respectively.[18] The upper and lower signs refer to upper and lower P components, respectively, in each of the κ and μ stacks. The values of $2r$ and $2|w|$ correspond to the energy distances between vibronic levels as shown in Fig. 8(b) under the limiting conditions of $r \gg |w|$, $r \gg BJ$, and $|w| \gg BJ$. As suggested by Hougen, Eqs. (8) are similar to the well-known relationship derived by Hill and Van Vleck, $B_{\text{eff}} = B(1 \pm B/\bar{A})$.[18] Following Eqs. (7), β is evaluated to be 38.88° for the $v_2=2$ and $K=1$ vibronic levels from the ratio between the constants describing the Renner-Teller coupling and spin-orbit interaction in Table IV. The effective rotational constants determined in this study, $B_{\text{eff}}^{\kappa\Pi_{1/2}}$, $B_{\text{eff}}^{\kappa\Pi_{3/2}}$, and $B_{\text{eff}}^{\mu\Pi_{1/2}}$, then give the B rotational constant of the (020) $^2\Pi$ vibronic level, 0.2053(16) cm^{-1}, which obviously increases from that of the 0_0^0 band, 0.204 26 cm^{-1},[12] in the excitation of bending mode as expected.

For the $^2\Sigma$ vibronic level with $K=0$ in the $^2\Pi$ electronic state, Hougen derived Eq. (1) to express the rotational energy, which we used to analyze the rotational structure of the (010) κ $^2\Sigma^{(+)}$ vibronic level. He also showed that the $B_{\text{eff}}^{\kappa\Sigma}$ and $p^{\kappa\Sigma}$ constants in Eq. (1) were evaluated using his parameters, r and β, under the limiting case of $r \gg BJ$,[18]

$$B_{\text{eff}}^{\kappa\Sigma} = B\left\{1 + \frac{B}{2r}\cos^2 2\beta\right\}$$
$$p^{\kappa\Sigma} = 2B\sin 2\beta, \quad -2B < p^{\kappa\Sigma} < 2B.$$

Based on these expressions, the rotational constant, B, of the (010) κ $^2\Sigma^{(+)}$ vibronic level is calculated to be 0.2049 cm^{-1}, from $\beta=36.47°$ for the $v_1=1$ and $K=0$ vibronic levels. The order of the effective rotational constants determined, $B_{\text{eff}}^{(020)} > B_{\text{eff}}^{(010)} > B_{\text{eff}}^{(000)}$, is consistent with the general trend on the bending mode, and the intervals are also consistent with the expected value from the general expression of the vibrational-rotation α constant, $\sim B_e^2/\omega_2$. The $p^{\mu\Sigma}$ constant is evaluated to be 0.3917 cm^{-1}, which is in good agreement with the experimental value, 0.3593 cm^{-1}, listed in Table I. The (010) κ $^2\Sigma^{(+)}$ vibronic level might show the P-type doublings by the Coriolis interaction with the (020) $^2\Pi$ vibronic level. However, this effect would be hidden by much larger

TABLE V. The vibronic level energy of the bending vibronic bands of the $\tilde{A}\,^2\Pi$ state of MgNC(cm^{-1}).

		Analysis I[a]		Analysis II[a]		Analysis III[a]	
Vibronic level	Obs.	Calc.	Obs.−calc.	Calc.	Obs.−calc.	Calc.	Obs.−calc.
(020) κ $^2\Pi_{1/2}$	26 455.749	26 456.032	−0.283	26 455.336	0.413	26 455.628	0.121
(020) κ $^2\Pi_{3/2}$	26 447.571	26 448.831	−1.260	26 447.985	−0.413	26 447.681	−0.110
(020) μ $^2\Pi_{1/2}$	26 298.287	26 297.964	0.322	26 298.263	0.024	26 298.283	0.004
(010) κ $^2\Sigma^{(+)}$	26 290.641	26 288.146	2.495	26 290.667	−0.027	26 290.665	−0.024
(000) $^2\Pi$	26 084.229[b]	26 085.503	−1.274	26 084.227	0.003	26 084.221	−0.009

[a]See text.
[b]The band origin of the 0_0^0 band, T_0.

e/f splitting caused by the Renner-Teller and spin-orbit interactions, and absorbed into the $p^{\kappa\Sigma}$ constant.

B. The Coriolis interaction between the (020) $\mu\,^2\Pi_{1/2}$ and (010) $\kappa\,^2\Sigma^{(+)}$ vibronic levels in the $\tilde{A}\,^2\Pi$ electronic state

The e/f splitting of the (020) $\mu\,^2\Pi_{1/2}$ vibronic level has been interpreted as the P-type doubling induced by the Coriolis interaction with the (010) $\kappa\,^2\Sigma^{(+)}$ vibronic level, and analyzed using Eq. (6). As shown in the Appendix, the energy separation between the e and f sublevels, ΔE_{ef}, is estimated from the following relations:

$$\Delta E_{ef} = \beta^{\mu\Pi}\left(J+\tfrac{1}{2}\right),$$

$$\beta^{\mu\Pi} = (\sin\beta)p^{\mu\Pi},$$

where the constant $p^{\mu\Pi}$ is expressed as follows:

$$p^{\mu\Pi} = B_{v_2^2 v_2^1}\frac{4(g_{1,|1|})^2}{\Delta E_{\mu\Pi\Sigma}},$$

$$B_{v_2^2 v_2^1} = \langle v_2 = 2, l = 0|B|v_2 = 1, l = 1\rangle,$$

where $g_{1,|1|}$ is one of the matrix elements of the **G**-uncoupling operator in Eqs. (A1) and (A2), $\Delta E_{\mu\Pi\Sigma}$ is the distance between the (020) $\mu\,^2\Pi_{1/2}$ and (010) $\kappa\,^2\Sigma^{(+)}$ vibronic levels, and $B_{v_2^2 v_2^1}$ is the off-diagonal element of the B constants between the $|v_2=2,\ l=0\rangle$ and $|v_2=1,\ l=1\rangle$ levels. We have roughly estimated $B_{v_2^2 v_2^1}(g_{1,|1|})^2$ from the square root of the q_{v_2} constant for the l-type doubling,[22,33]

$$B_{v_2^2 v_2^1}(g_{1,|1|})^2 = \sqrt{q_{v_2}},$$

$$q_{v_2} = \frac{2B_e^2}{\omega_2}\left\{1 + 4\sum_{k=1,3}\zeta_{2k}^2\frac{\omega_2^2}{\omega_k^2-\omega_2^2}\right\}.$$

From the experimental results, $\omega_2 = 154\ \mathrm{cm}^{-1}$ in Table IV, $\beta = 38.88°$ at the $v_2=2$ and $K=1$ vibronic levels, $\Delta E_{\mu\Pi\Sigma} = 7.596\ \mathrm{cm}^{-1}$ derived from the $T_{v'}$'s, and adopting $B_0 = 0.204\,26\ \mathrm{cm}^{-1}$ (Ref. 12) as B_e, the $\beta^{\mu\Pi}$ constant is evaluated to be $-0.0077\ \mathrm{cm}^{-1}$, where we have neglected the Coriolis terms in q_{v_2}, i.e., have assumed $\zeta_{2k}=0$. The order of this roughly estimated value is in agreement with our experimental value, $-0.0162\ \mathrm{cm}^{-1}$, providing an evidence for our interpretation that the e/f doubling of the (020) $^2\Pi_{1/2}$ level originates from the Coriolis interaction with the (010) $\kappa\,^2\Sigma^{(+)}$ level. It should be noted that the (020) $\kappa\,^2\Pi$ level is also influenced by the Coriolis interaction. However, it lies by about $105\ \mathrm{cm}^{-1}$ above the perturber, (010) $\kappa\,^2\Sigma^{(+)}$, and the larger energy separation, $\Delta E_{\kappa\Pi\Sigma} \gg \Delta E_{\mu\Pi\Sigma}$, makes the effect indiscernible in the (020) $\kappa\,^2\Pi$ level under our spectral resolution.

As will be seen in the Appendix, the $\beta^{\mu\Pi}$ constant is calculated adapting the Van Vleck transformation. This adaptation is valid for the Coriolis interaction between the (020) $\mu\,^2\Pi_{1/2}$ and (010) $\kappa\,^2\Sigma^{(+)}$ vibronic levels. The coupling terms responsible for the e/f splitting, having the order of $\sim 0.01\ \mathrm{cm}^{-1}$, is much smaller than the distance between the two coupling vibronic level, $\sim 8\ \mathrm{cm}^{-1}$. The close proximity of two coupling states is indispensable for making this small effect apparent in the spectrum.

There are some examples of spectral anomalies found in the bending vibronic states of linear molecules, where Renner-Teller interaction accidentally locates two vibronic states very closely.

The $\tilde{X}\,^2\Pi_{3/2}$ state of the NCS radical has the vibronic levels of (020) $\mu\,^2\Pi_{3/2}$ and (010) $^2\Delta_{3/2}$ lying by $\sim 17\ \mathrm{cm}^{-1}$ apart. Their energy levels were shifted to repel each other in the opposite directions, and the interaction was found to follow the selection rules of $\Delta v_2 = \pm 1$, $\Delta J = 0$, and $\Delta P = 0$. This shift was interpreted as the second-order interaction of the Renner-Teller and spin-orbit couplings through a Σ^+ electronic state, and analyzed by the second-order spin-vibration coupling resulting from the $S^{\pm}G^{\mp}$ term.[34] We excluded this second-order effect, since this term has been included in the Hamiltonian for the P-type doubling in the first order.

In the $v_2=1$ bending vibrational level of the $\tilde{A}\,^2\Pi_u$ state of BO_2 (Ref. 35) and of the $\tilde{A}\,^2\Pi$ state of CaOH (and CaOD),[36] the $^2\Sigma$ and $^2\Delta$ vibronic components lie closely due to small Renner-Teller coupling. The e/f splittings of the rotational levels were interpreted as the K-type doubling induced by the K-type resonance which is literally the resonance between the same K vibronic levels. The K-type doubling is caused by the **G**-uncoupling operator and spin-vibration interaction with the selection rules of $\Delta l = \pm 1$. The interaction was then analyzed in terms of the second-order perturbation through a stretching vibronic level in the same electronic state following the $\Delta l = \pm 2$ selection rule. It is considered that this effect cannot be applied to analyze the (020) $\mu\,^2\Pi_{1/2}$ and (010) $\kappa\,^2\Sigma^{(+)}$ vibronic levels due to the selection rule.

The ground vibrational level of the $\tilde{X}\,^2\Pi$ state of C_3H and C_3D, that is, the $^2\Pi$ electronic level, shows the extraordinary large e/f splitting.[37] It was suggested to occur through the Coriolis interaction with the ν_4 $\mu\,^2\Sigma$ vibronic level arising from the ν_4 C–C–H bending motion in the $\tilde{X}\,^2\Pi$ state. Since this e/f splitting is caused by the interaction between the zero-point and bending vibrational levels, the evaluation of the coupling strength should be somewhat different from the present case. To calculate the interaction strength, the B constant in the ground vibrational level was used in the C_3H work. In contrast, we adopt the off-diagonal element of B between the $v_2=1$ and 2 vibronic levels, $\langle v_2^1=2,\ l=0|B|v_2^0=1,\ l=1\rangle$.

C. Band intensity

We were able to identify the v_2 vibronic bands; some of which showed some anomalies in the band intensities. The vibronic structure of these bands will be discussed in view of our knowledge obtained from the energy level analyses.

1. The vibronically allowed 2_0^2 $\kappa\,^2\Pi$ band

We have observed both of the $P' = \frac{1}{2}$ and $=\frac{3}{2}$ spin components in the 2_0^2 $\kappa\,^2\Pi$ band. The P-type doubling was not resolved under our spectral resolution, indicating the unim-

portance of the Coriolis interaction with the (010) $^2\Sigma$ vibronic level for understanding the vibronic structure of the 2_0^2 $\kappa\,^2\Pi$ vibronic level. The wave functions of the $P'=\frac{1}{2}$ and $=\frac{3}{2}$ vibronic levels can then be approximated by the linear combinations of the case (a) basis functions with $l=0$ and 2 within each of the $P'=\frac{1}{2}$ and $=\frac{3}{2}$ components, $|v_2',l';J',P';e/f$ parity$\rangle$. For the e parity components, they are written under the limiting conditions of $r \gg |w|$, $r \gg BJ$, and $|w| \gg BJ$, according to the formulation proposed by Hougen;[18]

$$\begin{aligned}|\tilde{A}(020)\kappa\,^2\Pi_{3/2};e\rangle &= \cos\beta\left|2,0;J',\tfrac{3}{2};e\right\rangle \\ &\quad + \sin\beta\left|2,2;J',\tfrac{3}{2};e\right\rangle, \\ |\tilde{A}(020)\kappa\,^2\Pi_{1/2};e\rangle &= \sin\beta\left|2,0;J',\tfrac{1}{2};e\right\rangle \\ &\quad + \cos\beta\left|2,2;J',\tfrac{1}{2};e\right\rangle,\end{aligned} \tag{9}$$

where β is one of the Renner-Teller parameters defined in Eq. (7). The wave functions of the f parity components have the same forms, and are degenerate with the e components without the Coriolis interaction. In the transitions originating from the vibrationless level with $l''=0$ of the $\tilde{X}\,^2\Sigma^+$ state, the transition moment arises from the $l'=0$ component of the $\tilde{A}\,^2\Pi$ state obeying the $\Delta l=0$ selection rule. Therefore, assuming $\langle \tilde{A}\,^2\Pi;l'=0,P'=\frac{1}{2}\left|\hat{\mu}_e\right|\tilde{X}\,^2\Sigma^+;l''=0\rangle = \langle \tilde{A}\,^2\Pi;l'=0,P'=\frac{3}{2}\left|\hat{\mu}_e\right|\tilde{X}\,^2\Sigma^+;l''=0\rangle$, the intensity ratio between the 2_0^2 $\kappa\,^2\Pi_{1/2}$ and $^2\Pi_{3/2}$ bands is predicted to be $\sin^2\beta:\cos^2\beta = 1:1.53$, where $\beta=38.88°$. This result is consistent with the observed intensity ratio of $I_{^2\Pi_{1/2}}:I_{^2\Pi_{3/2}} \approx 1:1.5$.

2. The vibronically allowed 2_0^2 $\mu\,^2\Pi$ band

The 2_0^2 $\mu\,^2\Pi$ vibronic level splits into two components, $\mu\,^2\Pi_{3/2}$ and $\mu\,^2\Pi_{1/2}$, by the Renner-Teller and spin-orbit interactions, both of which components are vibronically allowed to be combined with the vibrationless level of the $\tilde{X}\,^2\Sigma^+$ state. However, only the $\mu\,^2\Pi_{1/2}$ band is identified to occur in the spectrum.

As described in the Appendix, two P components, $P'=\frac{1}{2}$ and $=\frac{3}{2}$ in the 2_0^2 μ vibronic level, couple with each other by the Coriolis interaction through the (010) $^2\Sigma$ vibronic level. From the matrix elements shown in the Appendix, the coupling strength of the e component is evaluated as follows:

$$\begin{aligned}&\langle \tilde{A}(020)\mu\,^2\Pi_{1/2};e|H'|\tilde{A}(020)\mu\,^2\Pi_{3/2};e\rangle \\ &= -B_{v_2^2v_2^1}\frac{2(g_{1,|1|})^2}{\Delta E_{\mu\Pi\Sigma}}J\sqrt{\left(J-\frac{1}{2}\right)\left(J+\frac{3}{2}\right)}\sin\beta\cos\beta \\ &= -p^{\mu\Pi}J\sqrt{\left(J-\frac{1}{2}\right)\left(J+\frac{3}{2}\right)}\sin\beta\cos\beta \\ &= -\beta^{\mu\Pi}J\sqrt{\left(J-\frac{1}{2}\right)\left(J+\frac{3}{2}\right)}\cos\beta = C_\mu^e,\end{aligned} \tag{10}$$

where the f component has the same strength as that of e. The $P'=\frac{1}{2}$ and $=\frac{3}{2}$ components are then mixed with each other within the (020) $\mu\,^2\Pi$ level, and the wave functions of the two P components derived by first-order perturbation are the following:

$$\begin{aligned}&|\tilde{A}(020)\mu\,^2\Pi_{3/2};e\rangle \\ &\quad = \sin\beta|2,0;J',\tfrac{3}{2};e\rangle + \cos\beta|2,2;J',\tfrac{3}{2};e\rangle \\ &\qquad - \frac{C_\mu^e}{\Delta E_{\mu\Pi\Sigma}}\{\cos\beta|2,0;J',\tfrac{1}{2};e\rangle + \sin\beta|2,2;J',\tfrac{1}{2};e\rangle\}, \\ &|\tilde{A}(020)\mu\,^2\Pi_{1/2};e\rangle \\ &\quad = \cos\beta|2,0;J',\tfrac{1}{2};e\rangle + \sin\beta|2,2;J',\tfrac{1}{2};e\rangle \\ &\qquad + \frac{C_\mu^e}{\Delta E_{\mu\Pi\Sigma}}\{\sin\beta|2,0;J',\tfrac{3}{2};e\rangle + \cos\beta|2,2;J',\tfrac{3}{2};e\rangle\},\end{aligned}$$

where C_μ^e is the matrix element of Eq. (10). Only the $l'=0$ components in $|\tilde{A}\mu\,^2\Pi_{1/2}\rangle$ and $|\tilde{A}\mu\,^2\Pi_{3/2}\rangle$ only have nonzero values for the transition moments optically combined with the vibrationless vibronic level of the $\tilde{X}\,^2\Sigma^+$ state. Assuming $\langle \tilde{A}\,^2\Pi;l'=0,P'=\frac{1}{2}\left|\hat{\mu}_e\right|\tilde{X}\,^2\Sigma^+;l''=0\rangle = \langle \tilde{A}\,^2\Pi;l'=0,P'=\frac{3}{2}\left|\hat{\mu}_e\right|\tilde{X}\,^2\Sigma^+;l''=0\rangle$, we can evaluate the ratio of the transition moments between the $P'=\frac{1}{2}$ and $=\frac{3}{2}$ levels to be $\cos\beta+(C_\mu/\Delta E_{\mu\Pi\Sigma})\sin\beta:\sin\beta-(C_\mu/\Delta E_{\mu\Pi\Sigma})\cos\beta$. The value of $C_\mu/\Delta E_{\mu\Pi\Sigma}$ derived from our experimental results is estimated to be 0 to -0.2 in the range of $J=0.5-17.5$. It predicts that the intensity ratio between the rotational transitions of the $^2\Pi_{1/2}$ and $^2\Pi_{3/2}$ bands decreases with an increase of J. This prediction partly leads to the missing of the $^2\Pi_{1/2}$ band at higher J levels, but it is insufficient to account for the anomaly of band intensities.

3. The vibronically forbidden 2_0^1 $\kappa\,^2\Sigma^{(+)}$ band

According to the selection rule of $\Delta l=0$, the 2_0^1 $\kappa\,^2\Sigma^{(+)}$ band is vibronically forbidden in the $\tilde{A}\,^2\Pi-\tilde{X}\,^2\Sigma^+$ electronically allowed electronic transition. However, it occurs in the spectrum with the intensity comparable to the other vibronically allowed band, such as the 2_0^2 $\kappa\,^2\Pi$ band, which is weaker by about one order of magnitude than the electronically allowed origin band, $\tilde{A}\,^2\Pi-\tilde{X}\,^2\Sigma^+$.

The principal mechanism causing this effect might be the Renner-Teller interaction, which mixes the levels with the same K values of the $\tilde{A}\,^2\Pi$ and $\tilde{X}\,^2\Sigma^+$ states. The intensity of the 2_0^1 $^2\Sigma$ band can then be estimated using the following equation in terms of the mixing ratio and the transition moment along the molecular axis;[38]

$$\langle \tilde{A}\,^2\Pi; v_2' = 1, l' = 1; K' = 0 | \hat{\mu}_z | \tilde{X}\,^2\Sigma^+; v_2'' = 0,$$

$$l'' = 0; K'' = 0 \rangle$$

$$= C_{\mathrm{dip}} \{ \langle \tilde{X}\,^2\Sigma^+ | \hat{\mu}_z | \tilde{X}\,^2\Sigma^+ \rangle - \langle \tilde{A}\,^2\Pi | \hat{\mu}_z | \tilde{A}\,^2\Pi \rangle \},$$

$$C_{\mathrm{dip}} = \langle \Pi | H'_{\mathrm{HT}} | \Sigma^+ \rangle / \Delta E_{\Pi-\Sigma}, \tag{11}$$

where H'_{HT} denotes the dipolar term of the effective vibronic Hamiltonian which is induced by the Herzberg-Teller interaction, and $\Delta E_{\Pi-\Sigma}$ is the energy separation between the $\tilde{A}\,^2\Pi$ and $^2\Sigma^+$ electronic states. The mixing coefficient, C_{dip}, is calculated from the relation $\epsilon_1 \omega_2 = \langle \Pi | H'_{\mathrm{HT}} | \Sigma^+ \rangle^2 / 2\Delta E_{\Pi-\Sigma}$ (Refs. 27 and 39) ; $C_{\mathrm{dip}} = 0.088$, using the relation $\epsilon_1 = (\epsilon - \epsilon_2)/(1-\epsilon)$ (Ref. 29) and assuming $\epsilon_2 = 0$. Since the adopted ϵ constant includes ϵ_2 which is the one derived from the quadrupolar term in the effective vibronic Hamiltonian,[27,29] the value of C_{dip} would be the upper limit of the mixing coefficient in this estimation, though the contribution of ϵ_2 would be expected to be small from the consideration of the g_4 constant, as described in Sec. IV A. The term in Eq. (11) is evaluated to be C_{dip}0.83 D from the permanent electric dipole moments determined experimentally, 5.308 and 6.138 D, for the $\tilde{A}\,^2\Pi$ and $\tilde{X}\,^2\Sigma^+$ states, respectively,[11] suggesting that the transition moment for the $2_0^1\ \kappa\,^2\Sigma^{(+)}$ is about 0.07 D at the maximum. By contrast, the transition dipole moment of the $\tilde{A}\,^2\Pi - \tilde{X}\,^2\Sigma^+$ transition can be estimated to be 3.47 D from the transition energy, 26 000 cm^{-1}, and the fluorescence lifetime, ~15 ns. The $2_0^1\ \kappa\,^2\Sigma^{(+)}$ band is then suggested to be at least by three orders of magnitude weaker than that of the origin band, which is inconsistent with our observation. However, it is consistent with our observation that the $2_0^1\ \mu\,^2\Sigma^{(-)}$ band has not been identified in our spectrum. The $2_0^1\ \kappa\,^2\Sigma^{(+)}$ band would borrow the intensity from the $2_0^2\,^2\Pi$ vibronically allowed transition through the Coriolis interaction. But the strength of this interaction is too weak to explain the occurrence of the $2_0^1\ \kappa\,^2\Sigma^{(+)}$ band, as discussed in Sec. IV C 2. We have no reasonable explanation for this problem at the present stage.

ACKNOWLEDGMENTS

The authors are thankful to Hiroshi Kohguchi, James K. G. Watson, and Anthony J. Merer for their useful comments. This research was partially supported by the Ministry of Education, Science, Sports and Culture, Grant-in-Aid for Scientific Research (C), 16510078, 2004.

APPENDIX: DERIVATION OF THE LEVEL ENERGIES OF THE $^2\Pi$ VIBRONIC STATES

The e/f splitting observed in the rotational levels of the (020) $\mu\,^2\Pi_{1/2}$ vibronic state was interpreted as the P-type doubling caused by the Coriolis interaction with the vibronic level of (010) $\kappa\,^2\Sigma^{(+)}$ lying nearby. In the rotational Hamiltonian, H_{rot} of Eq. (3), the **G**-uncoupling operator and spin-vibration interaction induced the Coriolis interaction, and thus we introduced the perturbation Hamiltonian of Eq. (5) to take account of this effect. The evaluation of their matrix elements was essentially the same as that for the Λ-type doubling of $^2\Pi$ electronic state,[16,17,21,40] and we took the following four case (a) basis functions for each of the (020) $^2\Pi$ vibronic level with $l=0$ and 2;

$|v_2, l; J, P, \Lambda, \Sigma\rangle$:

$$\left|2,0;J,\tfrac{1}{2},1,-\tfrac{1}{2}\right\rangle, \quad \left|2,0;J,-\tfrac{1}{2},-1,\tfrac{1}{2}\right\rangle,$$

$$\left|2,0;J,\tfrac{3}{2},1,\tfrac{1}{2}\right\rangle, \quad \left|2,0;J,-\tfrac{3}{2},-1,-\tfrac{1}{2}\right\rangle,$$

and

$|v_2, l; J, P, \Lambda, \Sigma\rangle$:

$$\left|2,2;J,\tfrac{1}{2},-1,-\tfrac{1}{2}\right\rangle, \quad \left|2,-2;J,-\tfrac{1}{2},1,\tfrac{1}{2}\right\rangle,$$

$$\left|2,2;J,\tfrac{3}{2},-1,\tfrac{1}{2}\right\rangle, \quad \left|2,-2;J,-\tfrac{3}{2},1,-\tfrac{1}{2}\right\rangle,$$

respectively. For the (010) $^2\Sigma^{(+)}$ level, the following four case (a) basis functions have been adopted:

$|v_2, l; J, P, \Lambda, \Sigma\rangle$:

$$\left|1,-1;J,\tfrac{1}{2},1,\tfrac{1}{2}\right\rangle, \quad \left|1,-1;J,-\tfrac{1}{2},1,-\tfrac{1}{2}\right\rangle,$$

$$\left|1,1;J,\tfrac{1}{2},-1,\tfrac{1}{2}\right\rangle, \quad \left|1,1;J,-\tfrac{1}{2},-1,-\tfrac{1}{2}\right\rangle.$$

The ladder operators $J^{\pm}$ and $S^{\pm}$ in Eq. (5) are defined by

$$J^{\pm}|J,P\rangle = \sqrt{J(J+1) - P(P \mp 1)}\,|J, P \mp 1\rangle,$$

and

$$S^{\pm}|S,\Sigma\rangle = \sqrt{S(S+1) - \Sigma(\Sigma \pm 1)}\,|S, \Sigma \pm 1\rangle,$$

respectively. There are four kinds of the $G_{22}^{\pm}$ operator for $\Delta v_2 = \pm 1$ and $\Delta l = \pm 1$; G_{22}^{+}, G_{22}^{-}, $G_{22}^{+\dagger}$, and $G_{22}^{-\dagger}$ following the notation of Messiah.[42] For example, in the case of $\Delta v_2 = +1$, they hold the relation of Refs. 41 and 42,

$$G_{22}^{+}|v_2,l\rangle = \tfrac{1}{\sqrt{2}}\sqrt{v_2 + 1 + l + 1}\,|v_2 + 1, l + 1\rangle$$
$$= g_{v_2,l}^{+}|v_2 + 1, l + 1\rangle,$$

$$G_{22}^{-\dagger}|v_2,l\rangle = \tfrac{1}{\sqrt{2}}\sqrt{v_2 + 1 - l + 1}\,|v_2 + 1, l - 1\rangle$$
$$= g_{v_2,l}^{-\dagger}|v_2 + 1, l - 1\rangle, \tag{A1}$$

where $|v_2, l\rangle$ is the eigenfunction of doubly degenerate harmonic oscillator. The matrix elements are expressed as, for example, $g_{v_2,l}^{-\dagger}$ for the $G_{22}^{-\dagger}$ operator, the superscripts, such as $-\dagger$, of which identify the operator. The subscripts, such as v_2, l, express the quantum numbers, v_2 and l. The matrix element of the **G**-uncoupling operator, $J^{\pm}G_{22}^{\mp}$, which induces heterogeneous interaction, is as follows:

$$\langle v_2 + 1, l \pm 1; J, P \pm 1 | BJ^{\mp}G_{22}^{\pm} | v_2, l; J, P \rangle$$
$$= \langle v_2 + 1, l \pm 1 | B | v_2, l \rangle \langle v_2 + 1, l \pm 1 | G_{22}^{\pm} | v_2, l \rangle$$
$$\times \langle J, P \pm 1 | J^{\mp} | J, P \rangle$$
$$= B_{v_2^+ v_2} \tfrac{1}{\sqrt{2}} \sqrt{v_2 + 1 \pm l + 1}\,\sqrt{J(J+1) - P(P \pm 1)}$$
$$= B_{v_2^+ v_2} g_{v_2,l}^{\pm\dagger} \sqrt{J(J+1) - P(P \pm 1)}.$$

(a)

		$(020)\ ^2\Pi$				$(010)\ ^2\Sigma$			
		$\lvert 2,0;J,\frac{3}{2},1,\frac{1}{2}\rangle$	$\lvert 2,0;J,\frac{1}{2},1,-\frac{1}{2}\rangle$	$\lvert 2,0;J,-\frac{1}{2},-1,\frac{1}{2}\rangle$	$\lvert 2,0;J,-\frac{3}{2},-1,-\frac{1}{2}\rangle$	$\lvert 1,-1;J,\frac{1}{2},1,\frac{1}{2}\rangle$	$\lvert 1,-1;J,-\frac{1}{2},1,-\frac{1}{2}\rangle$	$\lvert 1,1;J,\frac{1}{2},-1,\frac{1}{2}\rangle$	$\lvert 1,1;J,-\frac{1}{2},-1,-\frac{1}{2}\rangle$
$(020)\ ^2\Pi$	$\langle 2,0;J,\frac{3}{2},1,\frac{1}{2}\rvert$	0	0	0	0	$-g^+_{1,-1}\sqrt{(J-\frac{1}{2})(J+\frac{3}{2})}$	0	$-g^{-\dagger}_{1,1}\sqrt{(J-\frac{1}{2})(J+\frac{3}{2})}$	0
	$\langle 2,0;J,\frac{1}{2},1,-\frac{1}{2}\rvert$	0	0	0	0	$g^+_{1,-1}$	$-g^+_{1,-1}(J+\frac{1}{2})$	0	$-g^{-\dagger}_{1,1}(J+\frac{1}{2})$
	$\langle 2,0;J,-\frac{1}{2},-1,\frac{1}{2}\rvert$	0	0	0	0	$-g^+_{1,-1}(J+\frac{1}{2})$	0	$-g^{-\dagger}_{1,1}(J+\frac{1}{2})$	$g^{-\dagger}_{1,1}$
	$\langle 2,0;J,-\frac{3}{2},-1,-\frac{1}{2}\rvert$	0	0	0	0	0	$-g^+_{1,-1}\sqrt{(J-\frac{1}{2})(J+\frac{3}{2})}$	0	$-g^{-\dagger}_{1,1}\sqrt{(J-\frac{1}{2})(J+\frac{3}{2})}$
$(010)\ ^2\Sigma$	$\langle 1,-1;J,\frac{1}{2},1,\frac{1}{2}\rvert$	$-g^+_{1,-1}\sqrt{(J-\frac{1}{2})(J+\frac{3}{2})}$	$g^+_{1,-1}$	$-g^+_{1,-1}(J+\frac{1}{2})$	0				
	$\langle 1,-1;J,-\frac{1}{2},1,-\frac{1}{2}\rvert$	0	$-g^+_{1,-1}(J+\frac{1}{2})$	0	$-g^+_{1,-1}\sqrt{(J-\frac{1}{2})(J+\frac{3}{2})}$				
	$\langle 1,1;J,\frac{1}{2},-1,\frac{1}{2}\rvert$	$-g^{-\dagger}_{1,1}\sqrt{(J-\frac{1}{2})(J+\frac{3}{2})}$	0	$-g^{-\dagger}_{1,1}(J+\frac{1}{2})$	0				
	$\langle 1,1;J,-\frac{1}{2},-1,-\frac{1}{2}\rvert$	0	$-g^{-\dagger}_{1,1}(J+\frac{1}{2})$	$g^{-\dagger}_{1,1}$	$-g^{-\dagger}_{1,1}\sqrt{(J-\frac{1}{2})(J+\frac{3}{2})}$				

(b)

		$(020)\ ^2\Pi$			
		$\lvert 2,0;J,\frac{3}{2},1,\frac{1}{2}\rangle$	$\lvert 2,0;J,\frac{1}{2},1,-\frac{1}{2}\rangle$	$\lvert 2,0;J,-\frac{1}{2},-1,\frac{1}{2}\rangle$	$\lvert 2,0;J,-\frac{3}{2},-1,-\frac{1}{2}\rangle$
$(020)\ ^2\Pi$	$\langle 2,0;J,\frac{3}{2},-1,\frac{1}{2}\rvert$	$\frac{(g^+_{1,-1})^2+(g^{-\dagger}_{1,1})^2}{\Delta E}(J-\frac{1}{2})(J+\frac{3}{2})$	$-\frac{(g^+_{1,-1})^2}{\Delta E}\sqrt{(J-\frac{1}{2})(J+\frac{3}{2})}$	$\frac{(g^+_{1,-1})^2+(g^{-\dagger}_{1,1})^2}{\Delta E}(J+\frac{1}{2})\sqrt{(J-\frac{1}{2})(J+\frac{3}{2})}$	0
	$\langle 2,0;J,\frac{1}{2},-1,-\frac{1}{2}\rvert$	$-\frac{(g^+_{1,-1})^2}{\Delta E}\sqrt{(J-\frac{1}{2})(J+\frac{3}{2})}$	$\frac{1}{\Delta E}\left\{\left((g^+_{1,-1})^2+(g^{-\dagger}_{1,1})^2\right)(J+\frac{1}{2})^2+(g^+_{1,-1})^2\right\}$	$-\frac{(g^+_{1,-1})^2+(g^{-\dagger}_{1,1})^2}{\Delta E}(J+\frac{1}{2})$	$\frac{(g^+_{1,-1})^2+(g^{-\dagger}_{1,1})^2}{\Delta E}(J+\frac{1}{2})\sqrt{(J-\frac{1}{2})(J+\frac{3}{2})}$
	$\langle 2,0;J,-\frac{1}{2},1,\frac{1}{2}\rvert$	$\frac{(g^+_{1,-1})^2+(g^{-\dagger}_{1,1})^2}{\Delta E}(J+\frac{1}{2})\sqrt{(J-\frac{1}{2})(J+\frac{3}{2})}$	$-\frac{(g^+_{1,-1})^2+(g^{-\dagger}_{1,1})^2}{\Delta E}(J+\frac{1}{2})$	$\frac{1}{\Delta E}\left\{\left((g^+_{1,-1})^2+(g^{-\dagger}_{1,1})^2\right)(J+\frac{1}{2})^2+(g^{-\dagger}_{1,1})^2\right\}$	$-\frac{(g^{-\dagger}_{1,1})^2}{\Delta E}\sqrt{(J-\frac{1}{2})(J+\frac{3}{2})}$
	$\langle 2,0;J,-\frac{3}{2},1,-\frac{1}{2}\rvert$	0	$\frac{(g^+_{1,-1})^2+(g^{-\dagger}_{1,1})^2}{\Delta E}(J+\frac{1}{2})\sqrt{(J-\frac{1}{2})(J+\frac{3}{2})}$	$-\frac{(g^{-\dagger}_{1,1})^2}{\Delta E}\sqrt{(J-\frac{1}{2})(J+\frac{3}{2})}$	$\frac{1}{\Delta E}\left\{\left((g^+_{1,-1})^2+(g^{-\dagger}_{1,1})^2\right)(J-\frac{1}{2})(J+\frac{3}{2})\right\}$

(c)

		$(020)\ ^2\Pi$			
		$\lvert 2,0;J,\frac{3}{2},f\rangle$	$\lvert 2,0;J,\frac{1}{2},f\rangle$	$\lvert 2,0;J,\frac{1}{2},e\rangle$	$\lvert 2,0;J,\frac{3}{2},e\rangle$
$(020)\ ^2\Pi$	$\langle 2,0;J,\frac{3}{2},f\rvert$	$\frac{2(g_{1,1})^2}{\Delta E}(J-\frac{1}{2})(J+\frac{3}{2})$	$-\frac{2(g_{1,1})^2}{\Delta E}(J+1)\sqrt{(J-\frac{1}{2})(J+\frac{3}{2})}$	0	0
	$\langle 2,0;J,\frac{1}{2},f\rvert$	$-\frac{2(g_{1,1})^2}{\Delta E}(J+1)\sqrt{(J-\frac{1}{2})(J+\frac{3}{2})}$	$\frac{2(g_{1,1})^2}{\Delta E}\{(J+1)^2+\frac{1}{4}\}$	0	0
	$\langle 2,0;J,\frac{1}{2},e\rvert$	0	0	$\frac{2(g_{1,1})^2}{\Delta E}\{J^2+\frac{1}{4}\}$	$\frac{2(g_{1,1})^2}{\Delta E}J\sqrt{(J-\frac{1}{2})(J+\frac{3}{2})}$
	$\langle 2,0;J,\frac{3}{2},e\rvert$	0	0	$\frac{2(g_{1,1})^2}{\Delta E}J\sqrt{(J-\frac{1}{2})(J+\frac{3}{2})}$	$\frac{2(g_{1,1})^2}{\Delta E}(J-\frac{1}{2})(J+\frac{3}{2})$

FIG. 9. The matrix elements of the **G**-uncoupling operator and the spin-vibration interaction for the $v_2'=2$ and $l'=0$ components of the $A\ ^2\Pi$ state. The basis functions are defined by the case (a) functions, $|v_2',l;J,P,\Lambda,\Sigma\rangle$, for (a) and (b), and the symmetrized case (a) functions, $|v_2',l;J,P,e/f\rangle$, for (c). See text for more details.

The matrix element for the spin-vibration homogeneous interaction, $S^{\pm}G^{\mp}_{22}$, is as follows:

$$\begin{aligned}
&\langle v_2+1,l\pm1;S,\Sigma\mp1|BS^{\mp}G^{\pm}_{22}|v_2,l;S,\Sigma\rangle \\
&\quad=\langle v_2+1,l\pm1|B|v_2,l\rangle\langle v_2+1,l\pm1|G^{\pm}_{22}|v_2,l\rangle \\
&\qquad\times\langle S,\Sigma\mp1|S^{\mp}|S,\Sigma\rangle \\
&\quad=B_{v_2^+v_2}\tfrac{1}{\sqrt{2}}\sqrt{v_2+1\pm l+1}\sqrt{S(S+1)-\Sigma(\Sigma\mp1)} \\
&\quad=B_{v_2^+v_2}g^{\pm\dagger}_{v_2,l}\sqrt{S(S+1)-\Sigma(\Sigma\mp1)}.
\end{aligned}$$

In the case of the Λ-type doubling, the **S**-uncoupling operator, $-J^{\mp}S^{\pm}$, is needed to be considered, but this term has been neglected in this treatment, because of the reason mentioned in Sec III C.

From these relations, we calculated the matrix elements of the perturbation Hamiltonian, Eq. (5), between the basis functions of the (020) $^2\Pi$ and (010) $^2\Sigma$ vibronic levels, as shown in Figs. 9 and 10 for $l=0$ and 2 of the Π level, respectively. Adopting the Van Vleck transformation, we can estimate the contribution of the (010) $^2\Sigma^{(+)}$ vibronic level to the elements of the (020) $^2\Pi$ level as shown in Figs. 9(a) and 10(a) for $l=0$ and 2 of the Π level, respectively.

To evaluate the off-diagonal matrix elements between the $^2\Pi$ and $^2\Sigma$ vibronic levels, the symmetrized wave functions generated through Wang-type matrix are used,

$$\begin{pmatrix}|J,P,f\rangle\\ |J,P,e\rangle\end{pmatrix}=\frac{1}{\sqrt{2}}\begin{pmatrix}-1 & 1\\ 1 & 1\end{pmatrix}\begin{pmatrix}|v_2,-l;J,-P,-\Lambda,S,-\Sigma\rangle\\ |v_2,l;J,P,\Lambda,S,\Sigma\rangle\end{pmatrix}.$$

Using the symmetrized wave function, the matrix elements of the (020) Π vibronic level are separated into the e and f parity components as shown in Figs. 9(c) and 10(c) for $l=0$ and 2 of the Π level, respectively. Here, we used the identity relation between $g^+_{1,-1}$ and $g^{-\dagger}_{1,1}$ derived from Eq. (A1) and they were defined to be $g_{1,|1|}$,

$$g^+_{1,-1}=g^{-\dagger}_{1,1}\ (=g^{+\dagger}_{2,0}=g^-_{2,0})\equiv g_{1,|1|}. \tag{A2}$$

On the basis of the matrix elements, it was concluded that the $l=0$ components of the Π level have the e and f parity components whose energy levels are described in the different J dependence [Fig. 9(c)]. Contrastingly, in the $l=2$ component, the matrix elements of the e and f components are completely the same with each other, and they were found to be degenerate [Fig. 10(c)]. The splitting energy, $\Delta E(v_2,l;J,P)$, between the e and f parity components attributed to the P-type doubling is thus evaluated by second-order perturbation using the matrix elements for the $l=0$ component as follows:

(a)

		(020) $^2\Pi$				(010) $^2\Sigma$			
		$\lvert 2,2;J,\frac{3}{2},-1,\frac{1}{2}\rangle$	$\lvert 2,2;J,\frac{1}{2},-1,-\frac{1}{2}\rangle$	$\lvert 2,-2;J,-\frac{1}{2},1,\frac{1}{2}\rangle$	$\lvert 2,-2;J,-\frac{3}{2},1,-\frac{1}{2}\rangle$	$\lvert 1,-1;J,\frac{1}{2},1,\frac{1}{2}\rangle$	$\lvert 1,-1;J,-\frac{1}{2},1,-\frac{1}{2}\rangle$	$\lvert 1,1;J,\frac{1}{2},-1,\frac{1}{2}\rangle$	$\lvert 1,1;J,-\frac{1}{2},-1,-\frac{1}{2}\rangle$
(020) $^2\Pi$	$\langle 2,2;J,\frac{3}{2},-1,\frac{1}{2}\rvert$		0	0	0	0	0	$-g^+_{1,1}\sqrt{(J-\frac{1}{2})(J+\frac{3}{2})}$	0
	$\langle 2,2;J,\frac{1}{2},-1,-\frac{1}{2}\rvert$	0		0	0	0	0	$g^+_{1,1}$	$-g^+_{1,1}(J+\frac{1}{2})$
	$\langle 2,-2;J,-\frac{1}{2},1,\frac{1}{2}\rvert$	0	0		0	$-g^{-\dagger}_{1,-1}(J+\frac{1}{2})$	$g^{-\dagger}_{1,-1}$	0	0
	$\langle 2,-2;J,-\frac{3}{2},1,-\frac{1}{2}\rvert$	0	0	0		0	$-g^{-\dagger}_{1,-1}\sqrt{(J-\frac{1}{2})(J+\frac{3}{2})}$	0	0
(010) $^2\Sigma$	$\langle 1,-1;J,\frac{1}{2},1,\frac{1}{2}\rvert$	0	0	$-g^{-\dagger}_{1,-1}(J+\frac{1}{2})$	0				
	$\langle 1,-1;J,-\frac{1}{2},1,-\frac{1}{2}\rvert$	0	0	$g^{-\dagger}_{1,-1}$	$-g^{-\dagger}_{1,-1}\sqrt{(J-\frac{1}{2})(J+\frac{3}{2})}$				
	$\langle 1,1;J,\frac{1}{2},-1,\frac{1}{2}\rvert$	$-g^+_{1,1}\sqrt{(J-\frac{1}{2})(J+\frac{3}{2})}$	$g^+_{1,1}$	0	0				
	$\langle 1,1;J,-\frac{1}{2},-1,-\frac{1}{2}\rvert$	0	$-g^+_{1,1}(J+\frac{1}{2})$	0	0				

(b)

		(020) $^2\Pi$			
		$\lvert 2,2;J,\frac{3}{2},-1,\frac{1}{2}\rangle$	$\lvert 2,2;J,\frac{1}{2},-1,-\frac{1}{2}\rangle$	$\lvert 2,-2;J,-\frac{1}{2},1,\frac{1}{2}\rangle$	$\lvert 2,-2;J,-\frac{3}{2},1,-\frac{1}{2}\rangle$
(020) $^2\Pi$	$\langle 2,2;J,\frac{3}{2},-1,\frac{1}{2}\rvert$	$\frac{(g^+_{1,1})^2}{\Delta E}(J-\frac{1}{2})(J+\frac{3}{2})$	$-\frac{(g^+_{1,1})^2}{\Delta E}\sqrt{(J-\frac{1}{2})(J+\frac{3}{2})}$	0	0
	$\langle 2,2;J,\frac{1}{2},-1,-\frac{1}{2}\rvert$	$-\frac{(g^+_{1,1})^2}{\Delta E}\sqrt{(J-\frac{1}{2})(J+\frac{3}{2})}$	$\frac{(g^+_{1,1})^2}{\Delta E}\{(J+\frac{1}{2})^2+1\}$	0	0
	$\langle 2,-2;J,-\frac{1}{2},1,\frac{1}{2}\rvert$	0	0	$\frac{(g^{-\dagger}_{1,-1})^2}{\Delta E}\{(J+\frac{1}{2})^2+1\}$	$-\frac{(g^{-\dagger}_{1,-1})^2}{\Delta E}\sqrt{(J-\frac{1}{2})(J+\frac{3}{2})}$
	$\langle 2,-2;J,-\frac{3}{2},1,-\frac{1}{2}\rvert$	0	0	$-\frac{(g^{-\dagger}_{1,-1})^2}{\Delta E}\sqrt{(J-\frac{1}{2})(J+\frac{3}{2})}$	$\frac{(g^{-\dagger}_{1,-1})^2}{\Delta E}(J-\frac{1}{2})(J+\frac{3}{2})$

(c)

		(020) $^2\Pi$			
		$\lvert 2,2;J,\frac{3}{2},f\rangle$	$\lvert 2,2;J,\frac{1}{2},f\rangle$	$\lvert 2,2;J,\frac{1}{2},e\rangle$	$\lvert 2,2;J,\frac{3}{2},e\rangle$
(020) $^2\Pi$	$\langle 2,2;J,\frac{3}{2},f\rvert$	$\frac{(g_{1,1})^2}{\Delta E}(J-\frac{1}{2})(J+\frac{3}{2})$	$-\frac{(g_{1,1})^2}{\Delta E}\sqrt{(J-\frac{1}{2})(J+\frac{3}{2})}$	0	0
	$\langle 2,2;J,\frac{1}{2},f\rvert$	$-\frac{(g_{1,1})^2}{\Delta E}\sqrt{(J-\frac{1}{2})(J+\frac{3}{2})}$	$\frac{(g_{1,1})^2}{\Delta E}\{(J+\frac{1}{2})^2+1\}$	0	0
	$\langle 2,2;J,\frac{1}{2},e\rvert$	0	0	$\frac{(g_{1,1})^2}{\Delta E}\{(J+\frac{1}{2})^2+1\}$	$-\frac{(g_{1,1})^2}{\Delta E}\sqrt{(J-\frac{1}{2})(J+\frac{3}{2})}$
	$\langle 2,2;J,\frac{3}{2},e\rvert$	0	0	$-\frac{(g_{1,1})^2}{\Delta E}\sqrt{(J-\frac{1}{2})(J+\frac{3}{2})}$	$\frac{(g_{1,1})^2}{\Delta E}(J-\frac{1}{2})(J+\frac{3}{2})$

FIG. 10. The matrix elements of the **G**-uncoupling operator and the spin-vibration interaction for the $v_2'=2$ and $l'=2$ components of the $\tilde{A}\,^2\Pi$ state. The basis functions are defined by the case (a) functions, $|v_2',l;J,P,\Lambda,\Sigma\rangle$, for (a) and (b), and the symmetrized case (a) functions, $|v_2',l;J,P,e/f\rangle$, for (c). See text for more details.

$$\begin{aligned}\Delta E\left(2,0;J,\frac{1}{2}\right) &= \mp B_{v_2^2v_2^1}\left\{\frac{2(g_{1,|1|})^2}{\Delta E_{\Pi\Sigma}}\left(J+\frac{1}{2}\right)\right.\\ &\quad\left.-\frac{4(g_{1,|1|})^2}{\Delta E_{\Pi\Sigma}C_E}\left(J-\frac{1}{2}\right)\left(J+\frac{1}{2}\right)\left(J+\frac{3}{2}\right)\right\}\\ &= \mp\frac{1}{2}\left\{p^\Pi\left(J+\frac{1}{2}\right)-q^\Pi\left(J-\frac{1}{2}\right)\left(J+\frac{1}{2}\right)\left(J+\frac{3}{2}\right)\right\},\end{aligned} \tag{A3}$$

$$\begin{aligned}\Delta E\left(2,0;J,\frac{3}{2}\right) &= \pm B_{v_2^2v_2^1}\frac{4(g_{1,|1|})^2}{\Delta E_{\Pi\Sigma}C_E}\left(J-\frac{1}{2}\right)\left(J+\frac{1}{2}\right)\left(J+\frac{3}{2}\right)\\ &= \pm\frac{1}{2}q^\Pi\left(J-\frac{1}{2}\right)\left(J+\frac{1}{2}\right)\left(J+\frac{3}{2}\right),\end{aligned}$$

where the upper and lower signs indicate the e and f sublevels, respectively. The term of $\Delta E_{\Pi\Sigma}$ is the separation between the $\mu\,^2\Pi_{1/2}$ and $\kappa\,^2\Sigma^{(+)}$ vibronic levels, and

$$B_{v_2^2v_2^1}=\langle v_2=2,l=0|B|v_2=1,l=1\rangle,$$

$$p^\Pi=B_{v_2^2v_2^1}\frac{4(g_{1,|1|})^2}{\Delta E_{\Pi\Sigma}},$$

$$q^\Pi=B_{v_2^2v_2^1}\frac{8(g_{1,|1|})^2}{\Delta E_{\Pi\Sigma}C_E},$$

$$C_E=3+\frac{1}{g_{1,|1|}^2}\Delta E_\Omega\Delta E_{\Pi\Sigma},$$

where ΔE_Ω is the energy spacing between $\Omega=\frac{1}{2}$ and $=\frac{3}{2}$ components. Since $(\Delta E_{\Pi\Sigma})^{-1}\gg(\Delta E_{\Pi\Sigma}C_E)^{-1}$, the q^Π term in Eq. (A3) would be neglected, and the e/f splitting in the $\Omega=\frac{3}{2}$ level is expected to be quite small. The zeroth-order wave functions, $|\kappa;J,P,e\rangle$, $|\mu;J,P,f\rangle$, etc., are expressed in terms of the symmetrized wave functions, $|l;J,P,e\rangle$, with $l=0$ and 2 for the e component,

$$\begin{pmatrix}|\kappa;J,P=1/2,e\rangle\\ |\mu;J,P=1/2,e\rangle\end{pmatrix}=\begin{pmatrix}\cos\beta & \sin\beta\\ -\sin\beta & \cos\beta\end{pmatrix}\begin{pmatrix}|2;J,P=1/2,e\rangle\\ |0;J,P=1/2,e\rangle\end{pmatrix}$$

and

$$\begin{pmatrix}|\kappa;J,P=3/2,e\rangle\\ |\mu;J,P=3/2,e\rangle\end{pmatrix}=\begin{pmatrix}\cos\beta & \sin\beta\\ -\sin\beta & \cos\beta\end{pmatrix}\begin{pmatrix}|0;J,P=3/2,e\rangle\\ |2;J,P=3/2,e\rangle\end{pmatrix}$$

for the $P=\frac{1}{2}$ and $=\frac{3}{2}$ components, respectively. The expressions are also evaluated for the f component, though they are not shown here. The term values of the upper levels of the (020) κ and $\mu\,^2\Pi_{1/2}$ band are thus expressed as follows:

$$F(\kappa\,^2\Pi_{1/2},J)=T_v+B_{\text{eff}}^{\kappa\Pi_{1/2}}J(J+1)\mp\tfrac{1}{2}(\cos\beta)p^{\kappa\Pi}\left(J+\tfrac{1}{2}\right),$$

$$p^{\kappa\Pi} = B_{v_2^2 v_2^1} \frac{4(g_{1,|1|})^2}{\Delta E_{\kappa\Pi\Sigma}}$$

and

$$F(\mu\ ^2\Pi_{1/2}, J) = T_v + B_{\text{eff}}^{\mu\Pi_{1/2}} J(J+1) \mp \tfrac{1}{2}(\sin\beta) p^{\mu\Pi}\left(J+\tfrac{1}{2}\right),$$

$$p^{\mu\Pi} = B_{v_2^2 v_2^1} \frac{4(g_{1,|1|})^2}{\Delta E_{\mu\Pi\Sigma}},$$

for κ and μ, respectively, where the upper and lower signs refer to the e and f sublevels, respectively. The term, $\Delta E_{\kappa\Pi\Sigma}$, in the $p^{\kappa\Pi}$ constant is the energy spacing between the (020) $\kappa\Pi$ and (010) $\kappa\Sigma^{(+)}$ vibronic levels, and $\Delta E_{\mu\Pi\Sigma}$ in $p^{\mu\Pi}$ is that between (020) $\mu\Pi$ and (010) $\kappa\Sigma^{(+)}$. These expressions indicate that the e/f splitting induced by the last term of the equations could occur in both of the κ and μ vibronic levels. However, the P-type splitting of the κ level is too small to be observed, because the κ level lies farther from $\Sigma^{(+)}$ than μ, i.e., $\Delta E_{\kappa\Pi\Sigma} \gg \Delta E_{\mu\Pi\Sigma}$. Finally, we can obtain the following expression for the term value of the upper level of the (020) $\mu^2\Pi_{1/2}$ level;

$$F(\mu\ ^2\Pi_{1/2}, J) = T_v + B_{\text{eff}}^{\mu\Pi_{1/2}} J(J+1) \mp \tfrac{1}{2}\beta^{\mu\Pi}\left(J+\tfrac{1}{2}\right),$$

where the upper and lower signs refer to the e and f sublevels, respectively.

[1] K. Kawaguchi, E. Kagi, T. Hirano, S. Takano, and S. Saito, Astrophys. J. **406**, L39 (1993).
[2] M. Guélin, J. Cernicharo, C. Kahane, and J. Gomez-Gonzalez, Astron. Astrophys. **157**, L17 (1986).
[3] R. R. Wright and T. A. Miller, J. Mol. Spectrosc. **194**, 219 (1999).
[4] M. Fukushima and T. Ishiwata, J. Mol. Spectrosc. **216**, 159 (2002).
[5] T. E. Odaka, T. Taketsugu, T. Hirano, and U. Nagashima, J. Chem. Phys. **115**, 1349 (2001).
[6] T. Taketsugu and S. Carter, Chem. Phys. Lett. **340**, 385 (2001).
[7] T. E. Odaka, T. Hirano, and P. Jensen, J. Mol. Spectrosc. **211**, 147 (2002).
[8] T. Hirano, K. Ishii, T. E. Odaka, and P. Jensen, J. Mol. Spectrosc. **215**, 42 (2002).
[9] T. E. Odaka, T. Hirano, and P. Jensen, J. Mol. Spectrosc. **216**, 379 (2002).
[10] O. Bludský, V. Špirko, T. E. Odaka, T. Hirano, and P. Jensen, J. Mol. Struct. **685–696**, 319 (2004).
[11] T. C. Steimle and R. R. Bousquet, J. Chem. Phys. **115**, 5203 (2001).
[12] M. Fukushima and T. Ishiwata, J. Mol. Spectrosc. **233**, 210 (2005).
[13] M. Fukushima and T. Ishiwata (unpublished).
[14] G. Herzberg, *Spectra of Diatomic Molecules* (Van Nostrand, Princeton, NJ, 1950).
[15] K. A. Walker and M. C. L. Gerry, J. Mol. Spectrosc. **189**, 40 (1998).
[16] H. W. Kroto, *Molecular Rotation Spectra* (Wiley, London, 1975).
[17] R. N. Zare, *Angular Momentum* (Wiley, New York, NY, 1988).
[18] J. T. Hougen, J. Chem. Phys. **36**, 519 (1962).
[19] C. H. Townes and A. L. Schawlow, *Microwave Spectroscopy* (McGraw-Hill, New York, NY, 1955).
[20] See EPAPS Document No. E-JCPSA6-127-030725 for assignments of the observed rotational transitions. This document can be reached via a direct link on the online article's HTML reference section or via the EPAPS homepage (http:www.aip.org/pubservs/epaps.html).
[21] J. H. Van Vleck, Phys. Rev. **33**, 467 (1929).
[22] A. J. Merer and J. M. Allegretti, Can. J. Phys. **49**, 2859 (1971).
[23] T. Oka, J. Chem. Phys. **47**, 5410 (1967).
[24] R. Renner, Z. Phys. **92**, 172 (1934).
[25] J. A. Pople, Mol. Phys. **3**, 16 (1960).
[26] C. Jungen and A. J. Merer, *The Renner-Teller Effect*, review article in Molecular Spectroscopy: Modern Research Vol. II, edited by K. N. Rao (Academic, New York, 1976).
[27] J. M. Brown, J. Mol. Spectrosc. **68**, 412 (1977).
[28] J. T. Hougen and J. P. Jesson, J. Chem. Phys. **38**, 1524 (1963).
[29] D. Gauyacq and Ch. Jungen, Mol. Phys. **41**, 383 (1980).
[30] J. M. Brown and F. Jørgensen, Mol. Phys. **47**, 1065 (1982).
[31] J. M. Brown and F. Jørgensen, Adv. Chem. Phys. **52**, 117 (1983).
[32] G. Herzberg, *Electronic Spectra of Polyatomic Molecules* (Van Nostrand Company, Princeton, NJ, 1967).
[33] H. H. Nielsen, Rev. Mod. Phys. **23**, 90 (1951).
[34] F. J. Northrup and T. J. Sears, Mol. Phys. **71**, 45 (1990).
[35] A. G. Adam, A. J. Merer, and D. M. Steunenberg, J. Chem. Phys. **92**, 2848 (1990).
[36] M. Li and J. A. Coxon, J. Chem. Phys. **102**, 2663 (1995).
[37] S. Yamamoto, S. Saito, H. Suzuki, S. Deguchi, N. Kaifu, and S. Ishikawa, Astrophys. J. **348**, 363 (1990).
[38] P. S. H. Bolman and J. M. Brown, Chem. Phys. Lett. **21**, 213 (1973).
[39] ϵ_1 is denoted as $\epsilon^{(2)}$ in Ref. 27, because it is the parameter in the second-order perturbational term. In Ref. 29, ϵ_1 corresponds to the parameter in the dipole term of the vibronic Hamiltonian, which occurs as the first term of the multipole expansion of the Hamiltonian.
[40] H. Léfèbvre-Brion and R. W. Field, *The Spectra and Dynamics of Diatomic Molecules* (Elsevier, San Diego, CA, 2004).
[41] W. Moffitt and A. D. Liehr, Phys. Rev. **106**, 1195 (1957).
[42] A. Messiah, *Quantum Mechanics*, translated from the French by G. M. Temmer (Elsevier Science, Amsterdam, The Netherlands, 1961), Vol. 1.